AD-A157 415 PROPERTIES OF A RETROGRESSED AND RE-AGED 7075 ALUMINUM 1/1
ALLOY(U) NAVAL AIR DEVELOPMENT CENTER WARMINSTER PA
AIRCRAFT AND CREW S.. E S TANKINS ET AL. 31 DEC 84
UNCLASSIFIED NADC-84096-60 F/G 11/6 NL

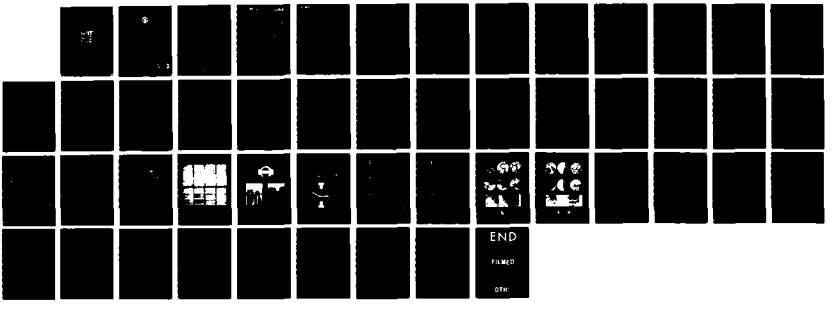

1.1
1.25
MICROCOPY RESOLUTION TEST CHART

REPORT NO. NADC-84096-60

PROPERTIES OF A RETROGRESSED AND RE-AGED 7075 ALUMINUM ALLOY

E. S. Tankins, V.S. Agarwala, C. E. Neu and J. J. Bethke
Aircraft and Crew Systems Technology Directorate (Code 606)
NAVAL AIR DEVELOPMENT CENTER
Warminster, Pennsylvania 18974

31 DECEMBER 1984

PROGRESS REPORT
AIRTASK ZF61-542-001
Work Unit No. ZM501

Approved for Public Release; Distribution is Unlimited

Prepared for
NAVAL AIR SYSTEMS COMMAND
Department of the Navy
Washington, DC 20361

NOTICES

REPORT NUMBERING SYSTEM – The numbering of technical project reports issued by the Naval Air Development Center is arranged for specific identification purposes. Each number consists of the Center acronym, the calender year in which the number was assigned, the sequence number of the report within the specific calender year, and the official 2-digit correspondence code of the Command Office or the Functional Directorate responsible for the report. For example: Report No. NADC-78015-20 indicates the fifteenth Center report for the year 1978, and prepared by the Systems Directorate. The numerical codes are as follows:

CODE	OFFICE OR DIRECTORATE
00	Commander, Naval Air Development Center
01	Technical Director, Naval Air Development Center
02	Comptroller
10	Directorate Command Projects
20	Systems Directorate
30	Sensors & Avionics Technology Directorate
40	Communication & Navigation Technology Directorate
50	Software Computer Directorate
60	Aircraft & Crew Systems Technology Directorate
70	Planning Assessment Resources
80	Engineering Support Group

PRODUCT ENDORSEMENT – The discussion or instructions concerning commercial products herein do not constitute an endorsement by the Government nor do they convey or imply the license or right to use such products.

APPROVED BY: _____ DATE: 6 May 1985

T. J. GALLAGHER
CAPT, MSC, U.S. Navy

Accession For	
NTIS GRA&I	X
DTIC TAB	☐
Unannounced	☐
Justification	
By	
Distribution/	
Availability Codes	
Dist	Avail and/or Special
A1	

UNCLASSIFIED

SECURITY CLASSIFICATION OF THIS PAGE (When Data Entered)

REPORT DOCUMENTATION PAGE

READ INSTRUCTIONS BEFORE COMPLETING FORM

1. REPORT NUMBER: NADC-84066-60	2. GOVT ACCESSION NO.: AD A157 415
3. RECIPIENT'S CATALOG NUMBER:	
4. TITLE (and Subtitle): Properties of a Retrogressed and Re-Aged 7075 Aluminum Alloy	5. TYPE OF REPORT & PERIOD COVERED: Progress Report
	6. PERFORMING ORG. REPORT NUMBER:
7. AUTHOR(s): E. S. Tankins, V. S. Agarwala, C. E. Neu & J. J. Bethke	8. CONTRACT OR GRANT NUMBER(s):
9. PERFORMING ORGANIZATION NAME AND ADDRESS: Naval Air Development Center, Aircraft & Crew Systems Technology Directorate (Code 606), Warminster, Pennsylvania 18974	10. PROGRAM ELEMENT, PROJECT, TASK AREA & WORK UNIT NUMBERS: AIRTASK ZF61-542-001, Work Unit No. ZM501
11. CONTROLLING OFFICE NAME AND ADDRESS: Naval Air Systems Command, Department of the Navy, Washington, DC 20361	12. REPORT DATE: 31 December 1984
	13. NUMBER OF PAGES: 42
14. MONITORING AGENCY NAME & ADDRESS(if different from Controlling Office)	15. SECURITY CLASS. (of this report): UNCLASSIFIED
	15a. DECLASSIFICATION/DOWNGRADING SCHEDULE:

16. DISTRIBUTION STATEMENT (of this Report)

Approved for Public Release; Distribution is Unlimited

17. DISTRIBUTION STATEMENT (of the abstract entered in Block 20, if different from Report)

18. SUPPLEMENTARY NOTES

19. KEY WORDS (Continue on reverse side if necessary and identify by block number)

~~Retrogression Re-aging; 7075-T651 Aluminum Alloy; Stress Corrosion Cracking; Exfoliation Corrosion~~, SEM Fractography, Differential Scanning Colorimetry, hardness, conductivity, fracture toughness, fatigue, and crack propagation.

20. ABSTRACT (Continue on reverse side if necessary and identify by block number)

Retrogression and Re-aging (RRA) is a new thermal process introduced for the purpose of enhancing corrosion resistance of 7075-T651 aluminum alloy while maintaining its T6 strength. In this study a 7075 material so treated was investigated for its mechanical and corrosion resistant properties.

Results indicated that the RRA treated 7075 was significantly better than the T6 temper in resistance to stress corrosion cracking and exfoliation corrosion. The loss in strength from

Over

DD FORM 1 JAN 73 1473 EDITION OF 1 NOV 65 IS OBSOLETE

S/N 0102-LF-014-6601

UNCLASSIFIED

SECURITY CLASSIFICATION OF THIS PAGE (When Data Entered)

20. ABSTRACT (Continued)

RRA treatment was minimal. Electron microscopy of the fractured surface showed a distinct difference in the fracture mode when compared to the T6 temper condition. Tests results indicated that the RRA heat treatment resulted in fatigue and fracture toughness properties superior to the 7075-T651. keywords :

front
1473

TABLE OF CONTENTS

LIST OF TABLES

LIST OF FIGURES

INTRODUCTION

Aluminum alloys of the 7000 Series (Al-Zn-Mg-Cu) have been used in airframe structures for over 25 years. The aluminum 7075 alloy, whose general chemical composition is given in Table 1, provides very high strength and stiffness in the T6 temper but is prone to exfoliation and stress corrosion cracking. The resistance to exfoliation and stress corrosion cracking can be improved by overaging to the T7 temper, but with a 10–15% loss of strength. The various time-temperature profiles for reaching the different tempers are listed in Table 2.

In 1974 a new thermal process was described (Reference a,b) for the 7075 Al alloy known as Retrogression and Reaging (RRA), which was reported to enhance the stress corrosion cracking (SCC) resistance of 7075–T6 while retaining the T6 mechanical properties. This process is applied to material in the T6 condition and consists of short time retrogression or partial solution treatment at a temperature in the range of 200–260°C (400–500°F), followed by water quenching and then reaging at the original aging temperature of 121°C (250°F). The exact temperature and time conditions were not given, but the general procedure of finding the desired conditions was outlined by Cina and Ranish (Reference a). These investigators believed that SCC was generally associated with the concentration of dislocations and the presence of undissolved $\eta\tau$ ($MgZn_2$) in the structure. They developed a thermal treatment to reduce the dislocation concentration and redissolve the excess η'. Cina suggested that the precipitation characteristics play an important role in improving SCC and the mechanical properties.

Recently there have been several excellent papers (Reference c–e) on the effect of precipitates on the properties of the 7000 Series aluminum alloys.

The results of the various investigators (Reference c–d) are all in agreement on the various mechanisms that are occurring in the 7075 alloys. They all reveal the existence of spherical Guinier preston (GP) zones, solute rich clusters and a transition phase η'. The precipitation sequence from a super saturated solid solution (SSS) condition is:

SSS - GP - η'' - η' - η @ Temp <190°C

SSS - GP - η'' - η' - $\eta + \tau$ @ Temp > 190°C

where;

GP is coherent

η'' is coherent

η' = ($MgZn_2$) is semi-coherent

η = ($MgZn_2$) is non-coherent

τ = $(Al, Zn)_{49}$ Mg_{32} is non-coherent

In terms of stability

$\tau > \eta > \eta' > \eta''$ > G.P. zones.

There have been very few attempts to quantatively correlate the microstructure to the various properties of the Al–Zn–Mg because of the complex precipitation process that occurs in these alloys. Ardell (Reference d) appears to present the most comprehensive characterization of the various precipitates.

The various precipitation mechanisms for the 7000 Series alloys have been discussed by Lorimer (Reference c). The solution treatment 480°C (890°F) results in a resolution of all the precipitates. The quench to room temperature results in a SSS. The SSS condition starts to form the coherent GP zones at room temperature. Artificial aging at 121°C (250°F) for 24 hrs. results in the formation of η'', η' plus some untransformed GP zones. The η' (semi-coherent) and the coherent GP zones are responsible for the T6 strength. The T7 overage results in η (non-coherent) and some η' (coherent) precipitates. The formation of the non-coherent precipitates results in a reduction of the mechanical properties and the increased SCC resistance characterized by the T7 temper. Duplex heat treatments have evolved to take advantage of various precipitate distributions.

Figure 1 shows schematically the effect of the time-temperature parametric treatment on the variations in hardness and/or yield strength observed during RRA (Reference a) treatment. During retrogression, hardness decreases to a minimum, increases again, going through a maximum, and then decreases as the material overages. On re-aging the strength is restored to over 95% of the original T6 level and has been shown to exceed the minimum T6 level (Reference g).

The most precise way to study the various reactions is to follow the changes in the precipitation reactions on a hot stage transmission electron microscope (TEM) along with the specific heat (C_p) associated with the various reactions.

There have been a few studies directed at the RRA Process (Reference d–g). They report excellent stress corrosion resistant properties with maintenance of the T6 strength level. Wallace et al (Reference g) suggest various promising heat treatment combinations starting wtih the T6 condition.

Whenever a material undergoes a change such as precipitation dissolution or reformation in the solid state, heat is either absorbed or liberated. These processes can be initiated by raising the temperature of the material. A relatively new experimental apparatus called the differential scanning calorimeter (DSC) has been designed to detect these heat changes. The DSC was designed to determine the enthalphies of these processes by measuring the differential heat flow required to maintain the temperature of the sample of the material and an inert reference at the same temperature. DSC is usually programmed to scan a temperature range by increasing linearly at a predetermined rate.

This technique was used to characterize the solid state reactions taking place in 7075. The investigators (References e and h) studied 7075-T651 and T7351 tempers and found that the high strength T651 (predominately GP zones) contained 3 regions defined as follows:
Region 1 – an endothermic reaction region at lower temperatures.
Region 2 – an exothermic reaction doublet at intermediate temperatures.
Region 3 – an endothermic reaction at higher temperatures. Their results (Reference e–h) are tabulated in Table 3.

The temperature at which the reaction is occurring at a maximum rate is defined as a peak reaction temperature, T_{PRT}, for a specific endotherm or exotherm.

The area of the specific endothermic or exothermic regions of the heat flow vs, temperature curves corresponds to the enthalphy associated with the reaction occurring over the temperature

range. These enthalphies can be utilized to study the various precipitaiton reactions occurring in the 7000 Aluminum alloy series.

The relative enthalphies and temperature limits of the various reactions are an indication of the density of the precipitates, size of the precipitate, volume fraction, and their type. Higher density and/or volume fraction (larger particles), require more heat. The relative degree of stability of a precipitate also determines the heat of solution.

The volume fraction and percent area coverage of grain boundaries of η and η' precipitates affects the fatigue, mechanical fracture toughness and SCC susceptibility of the 7075 alloy. The DSC thermograms are an indication of the amount of the precipitates, the temperature of the most rapid reaction, the temperature range over which the reaction occurs, and whether precipitates are being formed or dissolved. The thermograms can be related to the various tempers as well as changes in properties.

This investigation was undertaken to evaluate the fracture toughness, corrosion resistance and fracture behavior of RRA treated 7075. Further, it was felt that the DSC studies would be an excellent way to characterize RRA since the DSC results for 7075–T651 and 7075 T7351 have been well established.

EXPERIMENTAL PROCEDURE

MATERIAL

The material used in this investigation was 1 inch (25.4 mm) thick 7075–T651 aluminum plate obtained from Alcoa. The chemical composition and the different heat treatments are shown in Tables 1 & 2 (Reference a, b,e–1).

The NAVAIRDEVCEN furnished 12 pieces of 1 inch thick plate (25.4 mm) 7075 aluminum plate in several dimensions to Lockheed, California Co. to perform the RRA treatment, since at the time they had the exclusive US industrial license in accordance with the Israel Aircraft Industries Patent (Reference b and m). These samples were returned in the RRA condition to the NAVAIRDEVCEN and the initial heat treatment results reported (Reference m).

RRA PROCESSING

Lockheed reported (Reference m) that the retrogression treatment was performed in a molten salt bath to ensure rapid heating. They conducted experiments to find the most efficient mode of thermal treatment and the time for the material to reach the retrogression temperature. The retrogression time and temperature was proprietary; however, Cina (Reference a) reported times of 30–60 seconds at 250°C (482°F). All retrogressed plates were re-aged at 121°C (250°F) for 48 hours. A few retrogressed plates were re-aged for 96 hours to see if there was any further increase in hardness.

ELECTRICAL CONDUCTIVITY

Electrical conductivity tests were made using an eddy current conductivity meter, which gives conductivity values as a percentage of the international annealed copper standards (% IACS).

MECHANICAL PROPERTIES

Round tensile bars from the edge and the center locations of plate segments in both the T651 and RRA tempers were prepared and tested. Rockwell-B hardness was measured on the as-received T651 and on at least 1 plate in each heat treat group.

FATIGUE TEST METHODS

Fatigue Tests

R.R. Moore–type rotating beam fatigue tests (R3–1) were performed on unnotched specimens. The axis of the specimen was parallel to the roll direction of the plate (longitudinal) (Reference n).

Fatigue Crack Growth and Fracture Toughness

Fatigue crack growth rate measurements were made on compact tensile specimens (ASTM Standard E399) (Reference o) 2.4 inch (60.9 mm) x 2.5 inch (63.1 mm) by 1 inch thick (25.4 mm). The specimens were cycled on a 5000 lb (22,301N) capacity Krouse direct stress fatigue machine between loads of 250 lbs (1113N) minimum and 2300 lbs (10,235N) maximum (R = 0.11) until crack initiation was observed. The pre-cracked specimens were then cycled between loads of 150 and 1500 lbs (668 N and 6680 N) R = 0.10) at a frequency of 1 hertz on a MTS closed loop servohydraulic machine. Crack length measurements were taken at 1000 cycle intervals with a Gaertner optical micrometer until the cracks propagated to a length of approximately 1 inch (25.4 mm) from the load line. At this point fatigue cycling was terminated and the specimens were broken with a rising load for determination of plane strain fracture toughness (K_{IC}) in accordance with the ASTM test method E-399. Fatigue crack propagation rates were calculated by the seven-point incremental polynominal method described in ASTM test method E647 (Reference p).

CORROSION TEST METHODS

Exfoliaton Test

Exfoliation tests were performed on the stepped specimens of 7075–T651 and the RRA treated material in accordance with the ASTM G–34 Exco test (Reference q) for 48 hours (cf. Figure 4). The specimens were machined to expose the midplane (T/2) and also the T/4, T/8 and as rolled surfaces).

Stress Corrosion Tests

C-ring specimens as shown in Figure 5 evaluated in the study were taken from the short transverse direction of the plate. Specimens were machined from the 1 inch (25.4 mm) thick 7075–T651 and the RRA plates in accordance with reference (r).

The C-rings were loaded to stress levels of 15 ksi (103 MPa) and 25 ksi (172 MPa) in replicates of five and exposed in 3.5% NaC1 solution under alternate immersion conditions conforming to ASTM G-44 (Reference r). The duraction of the test was 30 days. The C-ring specimens were inspected for failures (cracks) periodically under 10X microscope when wet.

Double Cantilever Beam (DCB) Test

DCB specimens 1 inch (25.4 mm) x 1 inch (25.4 mm) x 5 inch (127 mm), were machined from 7075–T651 and RRA treated plates, having their length parallel to the rolling direction (SL orientation). The schematic of the specimen and its orientation are shown in Figure 6. The specimens were loaded through bolts in the short transverse direction until a crack formed at the root of the machined notch. The initial crack lengths and the load line displacements were used to calculate the stress intensities at fracture (K_c). The crack lengths were measured optically using a travelling microscope. The tests were performed in accordance with the procedure outlined by Hyatt (Reference t) and Sprowls et. al. (Reference u).

DIFFERENTIAL SCANNING CALORIMETRY (DSC)

The Differential Scanning Calorimetric (DSC) technique was utilized to characterize the various solid state reactions of precipitate dissolution and new precipitate formation. The deviations from a horizontal reference line are related to solid state reactions resulting from heating.

The calorimetric measurements were made using a DuPont 1090 thermal Analyzer containing a DSC module. Sample discs of approximately 7/32 in (0.56 cm) diameter x 0.050 in (0.127 cm) thickness were prepared and analyzed at the T651 temper, T651 + RRA, the T735 temper and T651 plus a T651 specimen heat related four hours at 180°C (356°F) and re-aged at 120°C for 24 hours. A pure aluminum disc was used as a reference. Runs were made at a heating rate of 10°C/min (18F) over the range from room temperature to 480°C (896°F). Dried nitrogen was passed through the calorimeter to minimize oxidation. The reference disc and the sample disc were prepared as close to the same weight as possible i.e. 50%. The calibration factor was frequently checked using pure aluminum as a standard and was modified to correct for instrument variation. The traces are based on calorimeter data that have been complemented by a temperature-dependent instrument calibration.

The use of the DSC method has been discussed in detail elsewhere (Reference h).

TRANSMISSION ELECTRON MICROSCOPE (TEM)

One-mm thick strips were cut from the specimens by a precision cut-off wheel. The thin foils for electron microscopy were prepared using discs 3 mm in diameter which had been punched from the strip after mechanically polishing to 0.13 mm in thickness. The discs were polished using twin jet electrolytic polishing to form microscopic perforations in the center of the faces.

The thinning was performed in an electrolyte of 20% HN_{03}, 80% CH_3OH with a current density of 100–500 ma/cm^2. The bath temperature was –30°C (–22°F). All the TEM was done at 100KV using a RCA EMV–3 electron microscope.

RESULTS

HARDNESS AND CONDUCTIVITY

Kaneco (Reference m) performed hardness, electrical conductivity, and tensile tests on each plate heat treated to the RRA condition. The data for the plates used to prepare the test specimens in this investigation are presented in Tables 4 and 5. Conductivity of all plates

was in the T76 range after the RRA heat treatments. The original hardness was nearly recovered. The increase in hardness for the 96 hours aging time appears insignificant.

TENSILE PROPERTIES

Table 4 shows results of the as-received 7075 plate and the 7075 T6 plate plus the RRA treatment. The T651 and T7 federal specifications are included (Reference m).

The RRA tensile properties are within the T651 specifications as shown by Table 4.

MICROSTRUCTURE

The basic microstructure of 7075–T651 plate consists of "Pancake-Shaped" grains which are almost equiaxed in two dimensions. These contain coarse iron and silicon rich inclusions which lie in stringers parallel to the rolling direction as shown in Figures 2 and 3 (Reference v). The grain shape and inclusion distribution are established during earlier processing and are not affected by the RRA treatment.

EXFOLIATION RESISTANCE

The exfoliation resistance of RRA treated specimens was significantly better than the original T651 condition. A comparative evaluation of the two thermal treatments can be made from Figure 4. The top row of RRA stepped specimens show only slight corrosion (some pitting) while the bottom row of T651 specimens show excessive lamellar corrosion. The appearance of the RRA specimens was similar to that of the T73 temper after exfoliation testing.

STRESS CORROSION RESISTANCE

In Table 6 a comparative evaluation of the C-ring stress corrosion tests is shown for the T651 and the RRA treatment. As was expected, none of the RRA specimens failed during this test of 30 days whereas the T651 specimens showed both cracking and intergranular corrosion. RRA specimens showed evidence of pitting (cf. Figure 5) but almost no intergranular corrosion. Photomicrographs of C-ring specimens at the high stress area show the details of this difference (Figure 5).

K_{ISCC} AND CRACK GROWTH RATES

The relationship between the crack growth rate (da/dt) and the stress intensity (K_I) during SCC was determined from the double cantilever beam test. The type specimen used is shown in Figure 6. The T651 and RRA treated specimens were tested in replicate in 3.5% NaCl solution at pH 6.5 and 2. The results are shown in Figures 7 and 8, respectively. It can be seen that at both test pH values the crack growth rate for the T651 temper was always much greater than that of the RRA temper. At high stress intensities, the crack growth rates for RRA were more than an order of magnitude lower. The threshold values (K_{ISCC}) of K_1 increased from about 5 MPa$\sqrt{m}$ (T651) to above 20 Mpa$\sqrt{m}$ (RRA). The K_{ISCC} value for the RRA specimens is not very well defined because crack growth rates below a few micron/hr are difficult to measure. In the T651 condition the K_{ISCC} value is very pronounced, as the da/dt vs K_1 plots have already shown a vertical slope (independent of K_1) at those low crack growth rates. The most sensitive direction for SCC is the short transverse with the crack propagating in the longitudinal (or rolling) direction. Appendix A contains all the test data including those tests (declared invalid) on specimens oriented improperly. Appendix A also describes the details of the DCB

test procedure for calculations of stress intensity and data reduction for the best parabolic fit of the curve da/dt vs K_1.

In the short transverse (S-L) direction in which the threshold stress intensities, K_{1scc}, are lowest, the stress corrosion cracking path is the shortest and the tensile stresses are practically perpendicular to the grain boundaries. Resolved stress components normal to grain boundaries increase the tendency to SCC.

The results are in agreement with Wallace et. al. (Reference g), who preferred DCB tests in a 3.5% NaCl sea water solution of 7075 material given an RRA type treatment. The trend of their data shows substantial improvement over T6 (Reference g. Wallace et. al.) Reference g also showed that lower temperatures and longer retrogression times could be utilized.

FRACTOGRAPHIC EXAMINATION

The DCB specimens were broken open after the termination of the corrosion tests and a small rectangular section was taken from the general area that was to be examined. Macrographs were made of the fracture surface area of interest. The fracture surfaces were examined for any unusual features and/or change of features.

Figures 9 and 10 are the representative fractographs of the RRA and T651 specimens. The macrographs shown in the rectangular section (cf. Figures 9 and 10) show the total profile of the fracture face from pre-crack to overload fracture. The micrographs (in circles) show the magnified views of the selected areas A, B and C. Area A represents the crack growth due to SCC, B the transition between the crack tip and the overload, and C the overload fracture.

In Figure 9, which depicts RRA treated specimens, the fracture mode contains dimple features (cf. circles A and B). This is characteristic of the behavior of ductile materials on fracture and typical of over-load fracture (Area C). The fracture morphology of the T651 specimens shown in Figure 10 is completely devoid of dimples in areas A and B. In particular area A showed mostly intergranular type of failure with severe corrosion. This is typical of brittle fracture. Area B which represents the transition region between SCC and overload shows dimples only in the overload part. Examination of the T651 specimen in the crack growth region to 1000X magnification did not reveal any dimples. The T651 specimen suffered major exfoliation attack, therefore fast SCC failure. A comparison of the two fractured lengths of the specimen faces in Figures 9 and 10 (extreme left photographs) also reveal this difference; the RRA crack length is much smaller than that of the T651.

The fracture surfaces of the T651 temper and the RRA fractured compact tension specimens were examined for any unusual or different features.

The optical microscope showed that the width of the precipitate free zones were the same. The SEM examination of the T651 and RRA material exhibited fatigue striations, microvoid coalescence and secondary cracking. The basic conclusion was that these features were the same for both tempers.

TRANSMISSION ELECTRON MICROSCOPE

A cursory examination of the thin films from the T651 and the RRA material revealed that the RRA material had larger and more abundant large precipitates than the T651. The T651 had a higher density of fine precipitates than the RRA material. These conclusions are qualitative with more work necessary to quantify the precise precipitate morphitogy.

DIFFERENTIAL SCANNING CALORIMETER

The DSC traces for the 7075–T651, RRA, T–7351 and a duplex heat treatment are shown in Figures 11–13 and the T_p (maximum reaction temp; or peak temp) and temperature range are summarized in Table 9. The most important characteristic of the DSC scans can be observed by comparing Figure 11 with 12 and 13. Figure 11 shows an exothermic doublet which has been analyzed in detail by other workers (Reference b). This doublet was called Region II. This region does not exist for RRA and T7351. Figure 12 shows that the T_p for Region I is greater for RRA than T651 (Figure 11). The T7351 has the highest T_p. The Figures 11–13 show that the region III is about the same for all the specimens.

FATIGUE PROPERTIES

Figures 14 and 15 show the results of the rotating beam fatigue tests for the RRA treatment. A scatter band for all 7075–T6 products (reference w) is also shown on Figure 14. Note that the RRA data falls in the middle of the band and thus is in good agreement with the 7075 results.

The data points of the rotating beam fatigue tests are tabulated in Tables 7 and 8. It can be seen that the fatigue behavior of T651 and RRA material appear similar. In the high stress region of the S–N fatigue RRA curve fell slightly below the T651 curve, reflecting the reduced strength level resulting from the treatment. The high cycle fatigue strength appears to be somewhat higher for the RRA treated material. Those results are in excellent agreement with Kaneko (Reference f).

FATIGUE CRACK GROWTH RATE

Plots of the Paris type power functions ($da/dn = c\,(\Delta k)\,m$) fitted to the fatigue crack growth rate test results are shown in Figure 16 and 17. These plots indicate that the crack growth rate is significantly slower for the RRA material than for the T651.

FRACTURE TOUGHNESS

Table 9 records the K_{IC} values for the 7075–T651 as-received material and the T651 and RRA treatment. The RRA K_{IC} values are slightly lower than the T651. Table 9 also contains the range of reported values (Reference x) for the T651 and T7351 temper in the LT and TL orientations. The RRA and T651 both fall within the lower limits of the reported values. The T651 temper in this investigation has a higher strength than the range of results in Table 6 so the K_{IC} would be expected to be somewhat lower. The RRA K_{IC} values are very close to the T651 as-received results and the T7351 K_{IC} range is higher, which is characteristic of the overaged lower strength material.

DISCUSSION

The results of the comprehensive study conducted by Ardell & Park (Reference o) will be very helpful in explaining the significant difference in the properties between 7075–T6 and the material given the RRA heat treatment. These authors analyzed T6, T7 and a series of specimens retrogressed at 240°C (464°F). The 60 second retrogressed specimen was re-aged. It appears likely that this is a similar precipitation mechanism in the presently reported study.

The results of Ardell & Park (Reference d) indicate the following:

(a) 7075–T651 consists of a low area (grain boundary) fraction covered by particles, a low mean particle size and high density.

(b) 7075–T76 consist of a large line (grain boundary) fraction, a large mean particle size and a low particle density.

(c) 7075–T651 + 30 seconds at 246°C (484°F) – re-aged at 121°C (250°F) for 48 hours consist of a line fraction and particle size similar to 7075–T76 and a low particle density. They point out that the matrix is made up of many very fine coherent η' particles and a large number of η particles.

Ardell and Park (Reference d) reported that a 7075–T651 sample subjected only to a retrogression treatment had similar grain boundary characteristics as the re-aged specimens. The grain boundary transformation appears to be very rapid. The re-aging resulted in the formation of very fine matrix precipitates believed to be η'.

Poulose et al (Reference y) in their stress corrosion cracking study showed that as the number of grain boundary precipitates decreases and as the area of grain boundary covered by precipitates increases, then the crack front velocity decreases. Microstructural features shown in their study are very similar to the results of Ardell & Park (Reference d). The significant observation from both studies is that SCC is related to the precipitate density on the grain boundary and the amount of the grain boundary line fraction covered. The larger precipitates and lower density result in a greater interparticle spacing, and the smaller precipitates and higher density have a shorter interparticle spacing. Adler (Reference z) showed that SCC was related to the interparticle spacing at a constant hardness and found 580A° or greater spacing resulted in minimum stress corrosion cracking.

There are several theories that attempt to explain stress corrosion cracking (Reference e). They are: (1) the grain boundary characteristic of the precipitate, (2) the matrix microstructure and (3) factors related to hydrogen embrittlement. The hydrogen embrittlement argument (Reference c) emphasizes the effects of magnesium segregated to grain boundaries. The magnesium segregation is non-equilibrium and is aided by vacancies during quenching. Aging allows for reestablishment of equilibrium by diffusion. Particles larger than a certain size act as nucleation sites for hydrogen bubbles, reducing the matrix hydrogen content and hence reducing the stress corrosion cracking. The results of this investigation indicated that the corrosion follows the grain boundaries and the susceptibility is controlled by the characteristics of the grain boundary precipitates. This does not exclude the other theories, but the grain boundary explanation seems the most feasible at the present. The grain boundary model makes the following assumptions (Reference l):

(a) The time-to-crack between precipitates is negligible compared to the electrochemical dissolution of precipitates.

(b) The precipitation free zone (PFZ) is not significant.

(c) The dissolution rate is a function of C/A where A is the anode area and C is the cathode area. The crack growth velocity depends on the dissolution rate.

Some of the microstructural feature discussed can be compared with the differential scanning calorimeter which picks up phase changes and/or formation and dissolution of precipitates.

DIFFERENTIAL SCANNING CALORIMETRY

The DSC characteristics of the microstructures produced in the RRA treatment appears to be similar to those of the T7 temper. The dissolution enthalphy, (area under the heat curves), for peak 1 in the RRA material (Figure 12) is greater and broader then the T651 material (Figure 11).

The most pronounced difference is the peak 11 (exothermic doublet peak) in Figure 11 for T651, which is absent for the RRA (Figure 12) and T7 (Figure 13). This indicates that the microstructure of T651 consists of some lower stability phases that are undergoing transformation. The T651 state appears to contain a stability coherent GP zone or η'' that transforms into the semi-coherent η' resulting in the exothermic peak.

The observation that peak I for the RRA treatment is broader and shifted to a higher temperature compared to T651 indicates either a larger particle size or a higher density of precipitates in its microstructure i.e. more heat is required to cause dissolution of particles. Further, since peak I for RRA falls between T6 and T7, it can be inferred that the RRA particle size is larger than the T6 but less then the T7. This is in general agreement with the results reported by Park and Ardell (Reference g).

The absence of the exothermic peak II indicates that the microstructure consists mainly of η' and η; otherwise there would be some η'' and η forming. Any significant formation of precipitates would result in an exothermic reaction. There may be some overlap with peak I or it may be a superposition of multiple dissolution peaks. There is a need for the clarification of the nature of the microstructures produced during aging treatments and an accurate placement of the phase boundaries. This would aid in further understanding the DSC result.

The T651 has a higher density of η' and a lower area coverage (Reference d). The SEM results in Figure 10 show that the corrosion fracture is intergranular for T651 and mixed mode for RRA as indicated in Figure 9. The DCB results shown in Figures 7–8 indicate that the crack growth rate is much slower for RRA than for T651. This is what would be expected from (a) and (c) above.

A careful optical examination was made of the microstructural features of the RRA and T651 DCB specimens, and no significant difference was observed in the precipitate free zone. Thus we ruled out the PFZ, which was thought to play a minor role, if any, in the properties examined in this investigation.

The fracture surfaces of T651 and RRA crack growth rate compact tension specimens were examined with similar results.

We can postulate a grain boundary model based on the C/A ratio which is as follows:

1) The smaller precipitates react quickly and act as stress intensifies under the tensile load to keep the crack confined to the grain boundary and growing at a higher velocity.

2) The larger precipitates react more slowly and tend to blunt the crack. The crack grows at a slower velocity and may become transgranular depending on the stress intensity.

Based on the experimental results and the grain boundary features it can be inferred that the C/A ratio is high in the T651, hence the crack velocity is greater, whereas the C/A

ratio is lower in RRA and T7, hence the crack velocity is slower.

The intergranular fracture mode is characterized by rapid crack advance while the slower crack growth may permit branching.

Another important characteristic that can be observed in Figures 11–13 is that for peak I, the harder T651 has the lowest Tr (Figure 11), whereas the softer T7 has the highest Tr (Figure 13). This is consistent with the concept that the strength comes from the myriad of fine coherent precipitates (lower energy to dissolve and/or transform) and the T7 state contains larger non-coherent precipitates (greater energy to dissolve and/or transform). The position of Tr appears to be consistent with the TEM features reported by Ardell (Reference d).

The large dissolution peaks that occur in all tempers (Figure 11–13) are definitely η since this is the only precipitate that can exist above 250°C (482°F).

FATIGUE CRACK GROWTH RATE

A detailed SEM examination was made of the fracture surface of the RRA material and the T651. There was no significant difference in the appearance of the fracture surfaces. The improved fatigue properties and the slower crack growth rate could not be attributed to secondary cracks (branching) or the width of the PFZ. These results are surprising since many earlier studies have shown such correlation (Reference bb). Another factor that may result in a slower crack growth rates is the surface free energy of the crack growth. The volume fraction of precipitates in RRA structure might result in a higher free energy of surface formation. This would require more stress to form a fresh crack surface and would result in a slower crack propegation. It is not clear what precipitate in the RRA structure is critical to the crack growth rate.

CONCLUSIONS

1. The RRA treatment provided considerable improvement to 7075–T651 1" plate in resistance to exfoliation and stress corrosion cracking.

2. The tensile properties of the RRA treated alloy are within the acceptable specifications of the T6 temper, but showed some loss of strength from the original.

3. The RRA heat treatment predominately converts the T6 microstructure to a more stable microstructure similar to T73, although further verifications are required.

4. The DSC results and the TEM cursory examination indicate that the major differences between the T6, RRA and T73 microstructures may be in the relative proportions of the GP zones, η' and η. The RRA material and the T7 temper DSC thermograms do not have an exothermal region 2. The T6 temper has an exothermal region thought to be related to the formation of η'.

5. The SEM fractographic features indicate an intergranular fracture mode for the DCB T651 specimens and a mixed mode for the RRA DCB specimen.

6. There is a 10% improvement in the high cycle fatigue strength of the RRA material over the as received 7075–T651.

7. There is a 10–15% reduction in the crack growth rate in the RRA material over the 7075–T651.

8. The KIC values are similar to the T651 with the RRA material slightly lower. The SEM microscopic examination of the fracture features failed to show any difference between the RRA and 7075–T651 material.

FUTURE PLANS

Since the results of this investigation look promising, future work is planned to explore the use of RRA treatment for thicker sections. Some TEM work is being planned to study the role of the various precipitates.

ACKNOWLEDGEMENTS

The authors appreciate the assistance of Messrs. E. Fogarty and W. Warden for the testing and Mr. W. Weist for the SEM work. The authors thank Dr. G. J. London for his many valuable suggestions and Mr. W. Frazier for his assistance and discussions on the TEM examinations.

REFERENCES

(a) B. Cina and B. Ranish, "New Technique for reducing Susceptibility to Stress. Corrosion of High Strength Aluminum Alloys", in Aluminum Industrial Products, Pittsburgh Chapter, American Society for Metals, 1974.

(b) United States Patent 3856584, 24 December 1974.

(c) G. W. Lorimer, "Precipitation in Aluminum Alloys" Proceedings of AIME Conference on Precipitation Processes in Solids, TMS–AIME, Warrendale, PA, pp 87–119, 1976.

(d) A. J. Ardell and J. K. Park, "Fundamental Investigation of the Retrogression and re-aging (RRA) of Commercial Al-base Alloys and its Effect on Stress Corrosion Cracking", UCLA School of Engineering and Applied Science. Contract No. N00014–81–K–0292, May, 1982.

(e) J. M. Papazian: "Effect of Two-Stage Aging on Microstructure of 7075 Aluminum Alloys RE–627, Dept. of the Navy. Contract No. N00019–79–C–0285, Grumman Aerospace Corp., Bethpage, New York, April 1981.

(f) R. S. Kaneko: "RRA Solution for Stress Corrosion Problems with T6 Temper Aluminum", Metals Progress, Vol 117, No. 5, p. 41, April 1980.

(g) W. Wallace, J. C. Beddes and M. C. DeMalherbe: "A New Approach to the Problem of Stress Corrosion Cracking in 7075–T6", National Aeronautical Establishment Report, Ottowa, Ontario, K1AOR6, Sept. 1981.

(h) R. Delasi and P. N. Adler: "Calorimetric Studies of 7000 Series Aluminum Alloys. I Matrix precipitate Characterization of 7075 & II. Comparison of 7075, 7050 and RX720" Met Trans. Vol 8A, p. 1177 and 1185, 1972.

(i) Military Specification: "Heat Treatment of Aluminum Alloys", MIL–H–6088E, 5 Feb. 1971.

(j) Aluminum Standards and Data 1974, The Aluminum Association, Inc., Sixth Edition, 1979.

(k) E. D. Russo, M. Conserva, F. Gatto, R. H. Markus: "Thermomechanical Treatments on High Strength Al-Zn-Mg(-ca) Alloys". Met Trans., Vol 4A, p. 1133, 1973.

(l) Alcoa Green Letter on 7075–T73 Aluminum Company of America, Sept. 1971.

(m) R. S. Kaneko: "Retrogression and Re-aging (RRA) of 7075–T651, 1–Inch Thick Plate", Supplement to Contract N67269–78–C–0446, LR29577, Aug, 1980.

(n) "Metals – Physical, Mechanical Corrosion testing", Part 10, ASTM Standards, Philadelphia, PA 1979.

(o) "Standard Test Method for Plane – Strain Fracture Toughness of Metallic Material". ANSI/ASTM E 399–74, Philadelphia, PA, p. 505, 1974.

REFERENCES (Continued)

(p) "Tentative Test Method for Constant-Load-Amplitude Fatigue Crack Growth Rates Above 10^{-8}m/cycle", ASTME 647-78 I, Philadelphia, PA 1978.

(q) ANSI/ASTM G 34, Standard Method of Test for Exfoliation Corrosion Susceptibility in 7xxx Series Copper Containing Aluminum Alloys (EXCO test). 1979 Annual Book of ASTM Standards part 10.

(r) ANSI/ASTM G 38–73. Making and Using the C-Ring Stress Corrosion Tracking Test Specimen. 1979 Annual Book of ASTM Standards.

(s) ANSI/ASTM G 44–75 Standard Recommended Practice for Alternate Immersion Stress Corrosion Testing in 3.5% Sodium Chloride Solution.

(t) M. V. Hyatt. "Use of Pre-Cracked Specimens in Stress Corrosion Testing of High Strength Aluminum Alloys", Corrosion NACE, Vol. 26, No. 11, p. 487, 1970.

(u) D. O. Sprowls, T. J. Summerson, G. M. Ugiansky, S. G. Epstein, and H.L. Craig, Jr., "Evaluation of a Proposed Standard Method of Testing for Susceptibility to Stress-Corrosion Cracking of High-Strength 7xxx Series Aluminum Alloy Products", Stress Corrosion–New Approaches ASTM STP 610, ASTM, 1976.

(v) A. Phillips, V. Kerlins, & B. V. Whitenson, "Electron Fractograph Hand Book", Air Force Materials Lab. Report No. ML–T–DR–64–416, 1965.

(w) Aerospace Structural Metals Handbook, Vol 3, Code 3207, Mechanical Properties Data Center, Dec. 1980.

(x) R. W. Hertzberg: Deformation and Fracture Mechanics of Engineering Materials, John Wiley and Son, New York, p. 369, 1976.

(y) P, K. Poulose, J. E. Morrall and A. J. McEvily/ "Stress Corrosion Crack Velocity and Grain Boundary Precipitates in an Al-Zn–Mg Alloys", Met Trans. Vol 5A, p. 1393, 1974.

(z) P. N. Adler, R. Delasi and G. Geschwind: "Influence of Microstructure on the Mechanical Properties of Stress Corrosion Susceptibility of 7075 Aluminum Alloys", Met Trans, Vol. 3A, p. 3191, 1972.

(aa) M. E. Fine, Met Trans A, Vol 6A, 1975, p. 625.

(bb) D. S. Thompson, ibid, p. 671.

TABLE 1
COMPOSITION LIMITS OF ALUMINUM ALLOY 7075
(MIL–A–22771C 25 August 1989)

Element	Weight Percent
Copper	1.2–2.0
Silicon	0.4
Iron	0.50
Manganese	0.30
Magnesium	2.1–2.7
Zinc	5.1–6.1
Chromium	0.18–0.35
Titanium	0.20
Other Element	0.05
Other Element Total	0.15
Aluminum	Remainder

TABLE 2
HEAT TREATMENT OF 7075 (Reference a,)

T6: Solution treat, quench and age 120°C/29 hours to peak strength.
QQ–A–250/12E requirements: 68 ksi (469 MPa) yield strength minimum and 78 ksi (538 MPa) tensile strength minimum.

RRA: Start with T6 retrogress at 220°C for 1 minute, quench re-age 120°C/24 hours to peak strength.
78 ksi (535 MPa) yield stength and 87 ksi (600 MPa) tensile strength.

T6: Solution treat, quench and 2 stage age (95°C/4 hours + 155°C/8 hours).

T6: Special: Solution treat, quench and 2 stage age (105°C/6 hours + 150°C/8 hours).

T7: Solution treat, quench and 2 stage over-age (110°C/8 hours +177°C (8 hours) to improve stress corrosion resistance. Yield strength and tensile strength 10–15 percent lower than T6.

TABLE 3
7075: REACTIONS IN REGIONS OF DSC (Reference e, h, z)

Temper	Region	Temperature Range °F (°C)	Predominant Reaction	Other Reactions
T651	1	235–423 (113–217)	G.P. Dissolution	η' formation, growth and dissolution
	2	423–520 (217–217)	–	η' formation, growth and dissolution
	3	520–385 (271–448)	η' Dissolution	–
T7351	1	327–473 (164–245)	η' Dissolution	η' formation and growth
	3	473–828 (245–442)	η' Dissolution	–

TABLE 4
TENSILE PROPERTIES OF 7075 ALUMINUM ALLOY PLATE

IDENTITY	TEMPER	0.2% offset *Yield Strength* ksi (MPa)	*Tensile Strength* ksi (MPa)	Elongation In 25.4 mm (1 in) %
9A–1X	T651	78 (540)	87 (600)	10
		78 (535)	87 (600)	14
61–A	T651	76.6 (528)	86 (593)	12
		76.8 (578)	86.2 (594)	12
6C–3	RRA	72.5 (500)	81.5 (562)	14
		72.5 (500)	862 (561)	14
9A–3	RRA	68 (467)	78 (540)	14
		69 (478)	80 (549)	14
QQ–A–250/12E	T651	68 (469) (Minimum)	78 (538) (Minimum)	7 (Minimum)
	T7	63 (430)	73 (500)	13

9A–1X and 61–A were taken from the as received plate.

6C–3 and 9A–3 were taken from the RRA treated material used in the tests reported in this report.

TABLE 5
HARDNESS AND CONDUCTIVITY

Group	In(mm)xIn(mm)xIn(mm)	Hardness (R_B) T651 Range	T651 Avg	T651 + RRA 250°F (121°C) – 48 hrs Range	48 hrs Avg	T651 + RRA 250°F (121°C) – 96 hrs Range	96 hrs Avg	Conductivity (% IACS) T651	T651 + RRA 250°F (121°C) 48 hrs	96 hrs
4	1"(25.4)x6"(132.4)x16"(406.5)	88.0–89.0	88.7	84.0–84.5	84.2	85.0–86.5	85.3	34.0	39.5	40.5
7	1"(25.4)x6"(132.4)x16"(406.5)	89.0–89.5	84.3	87.5–88.0	87.8	–	–	34.0	39.5	
8	1"(25.4)x6"(132.4)x16"(406.5)	88.5–89.5	88.8	86.5–87.5	87.0	–	–	33.8	39.5	
(Control) As Receive		89.0–90.0	89.5	–	–	–	–	34.0	–	–

TABLE 6
RESULTS OF 3.5% NaC1 ALTERNATE IMMERSION C-RING TESTS

HEAT TREATMENT	STRESS ksi (MPa)	FORMS OF CORROSION	S. C. C. FAILURE F/N
T651	15(103)	I.G. with cracks	2/5
T651	25(172)	I.G. with cracks	4/5
T651 + RRA	15(103)	Pitting, No. I.G.	0/5
T651 + RRA	25(172)	Pitting, No. I.G.	0/5

I.G. – Intergrannular Corrosion

F/N – Ratio of number of specimens failed to the number of specimens tested.

TABLE 7
REACTIONS OCCURRING AT VARIOUS TEMPERATURES DURING DSC ANALYSIS OF 7075 A1 ALLOY

TEMPER CONDITION	REGION	PEAK TEMP. T_R °F (°C)	TEMP. RANGE °F (°C)	Δ Hr j/g
	I	369(187)	309–410 (154–210)	05.71
T651	IIa	440(227)	410–540 (210–282)	5.33
	IIb	478(248)		
	III	784(418)	540–838 (282–448)	21.8
	I	397(203)	324–536 (162–280)	6.07
T651 plus RRA	III	784(418)	536–842 (280–450)	22.6
T7351	I	415(213)	331–531 (166–277)	6.64
	II	766(408)	531–828 (277–442)	27.5

TABLE 8
ROTATING BEAM FATIGUE PROPERTIES OF 7075–T651 ALUMINUM ALLOY

Specimens No.	Stress MPa	(KSI)	Cycles to Failure
A-1	345	(50)	58,000
A-2	276	(40)	364,000
A-3	207	(30)	3,321,000
A-4	173	(25)	7,856,000
A-5	138	(20)	24,522,000 (NF)
A-6	152	(22)	30,589,000
A-7	138	(20)	59,031,000 (NF)
A-8	145	(21)	37,658,000
A-9	124	(18)	75,345,000 (NF)
A-10	138	(20)	118,637,000 (NF)
Reruns			
A-5	414	(60)	41,000
A-8	449	(65)	10,000
A-10	414	(60)	10,000

TABLE 9
ROTATING BEAM FATIGUE PROPERTIES OF 7075–T651 PLUS RRA

Specimens No.	Stress MPa	Stress (KSI)	Cycles to Failure
R1	345	(50)	42,000
R2	276	(40)	185,000
R3	207	(30)	3,319,000
R4	173	(25)	26,262,000 (NF)
R5	186	(27)	11,423,000
R6	152	(22)	70,468,000 (NF)
R8	179	(26)	3,949,000
R9	159	(23)	75,213,000 (NF)
R10	138	(20)	49,565,000 (NF)
R11	165	(24)	40,642,000
R12	165	(24)	15,428,000
Reruns			
R4	414	(60)	18,000
R10	414	(60)	12,000
R6	449	(65)	11,000
R7	345	(50)	39,000

TABLE 10
FRACTURE TOUGHNESS K_{IC} OF 7075 ALUMINUM PLATE

Temper	LT Orientation K_{IC} KSIσ in (MPa$\sqrt{m}$)	TL Orientation K_{IC} KSI in (MPa$\sqrt{m}$)
T651	26.97(29.64)	23.02(25.29)
T651 Plus RRA	26.84(29.49)	22.69(24.94)
T651*	25.28(27.31)	23.26(25.28)
T7351*	38.32(31.35)	24.37(26.11)

*Reference (x)

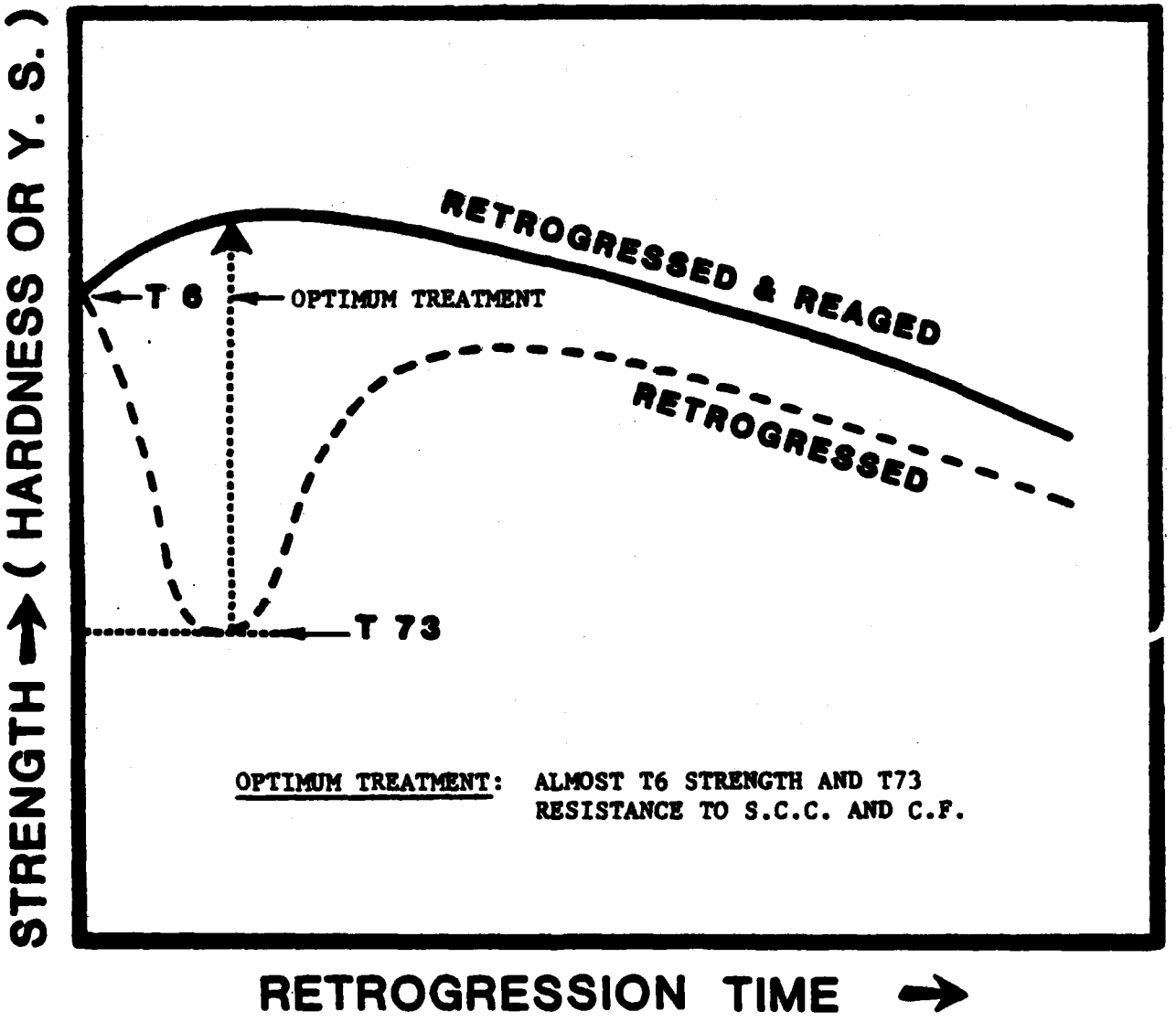

Figure 1. Schematic Representation of the Changes in Hardness or Strength During Retrogression and Re-Aging.

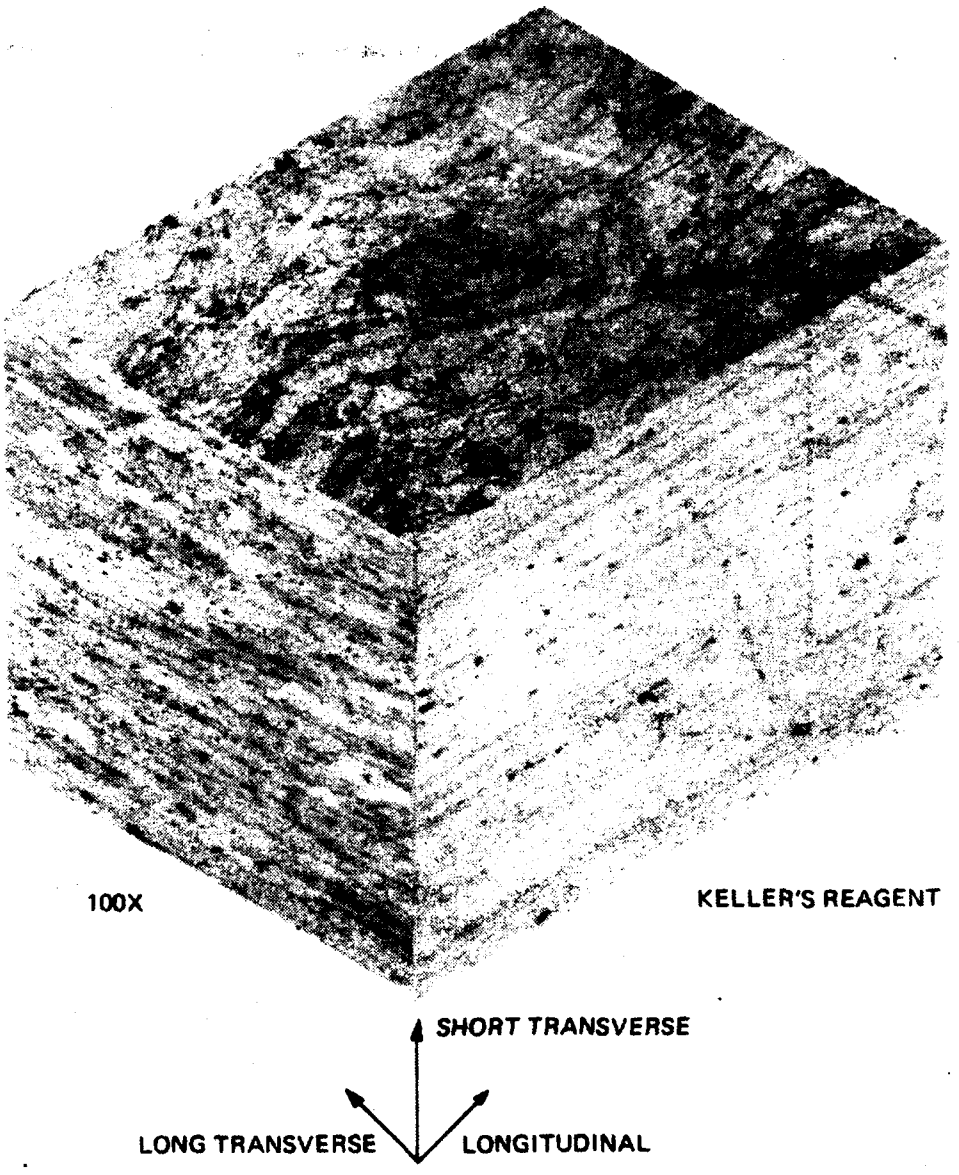

Figure 2. Microstructural Montage of 7075–T651 Aluminum Alloy.

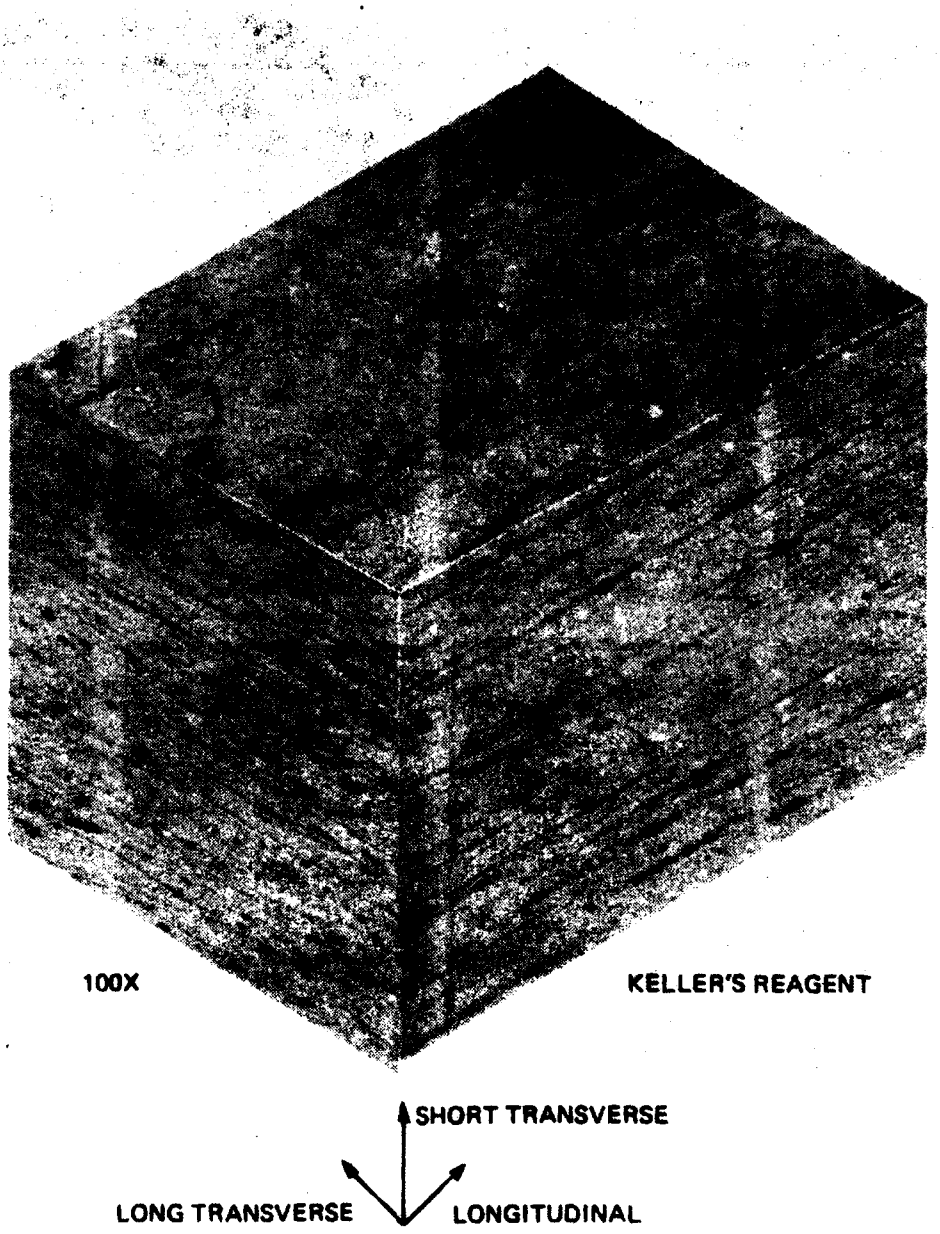

Figure 3, Microstructural Montage of 7075–T651 Plus RRA Heat Treatment.

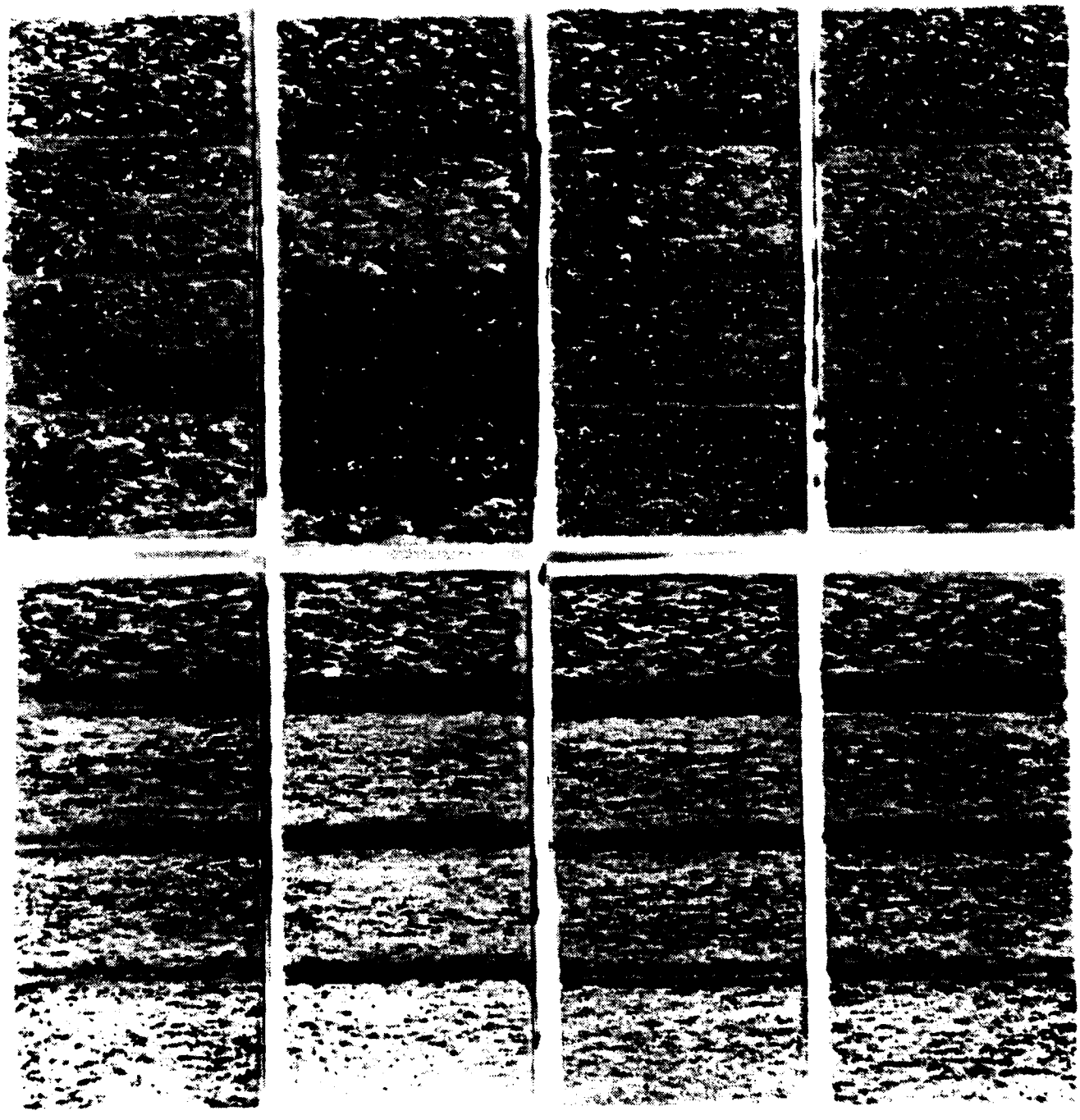

Figure 4. Comparison of Exposure Plates of 7075 A1 Alloy Tempered to T651 (Top Set) and T651 + RRA (Bottom Set). Conditions after Exfoliation Testing: The Thickness of the Plates Exposed are 1/2, 1/4, 1/8 and the Top Surface of Machined 1 Inch Plate.

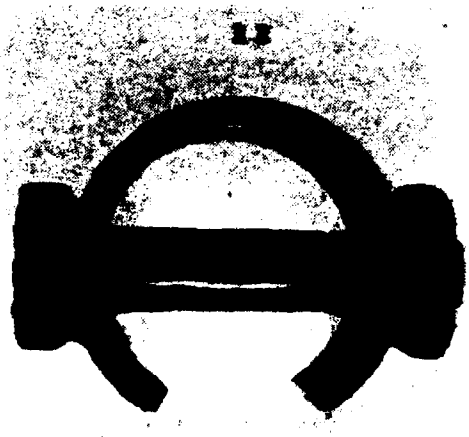

S C C C-RING TEST

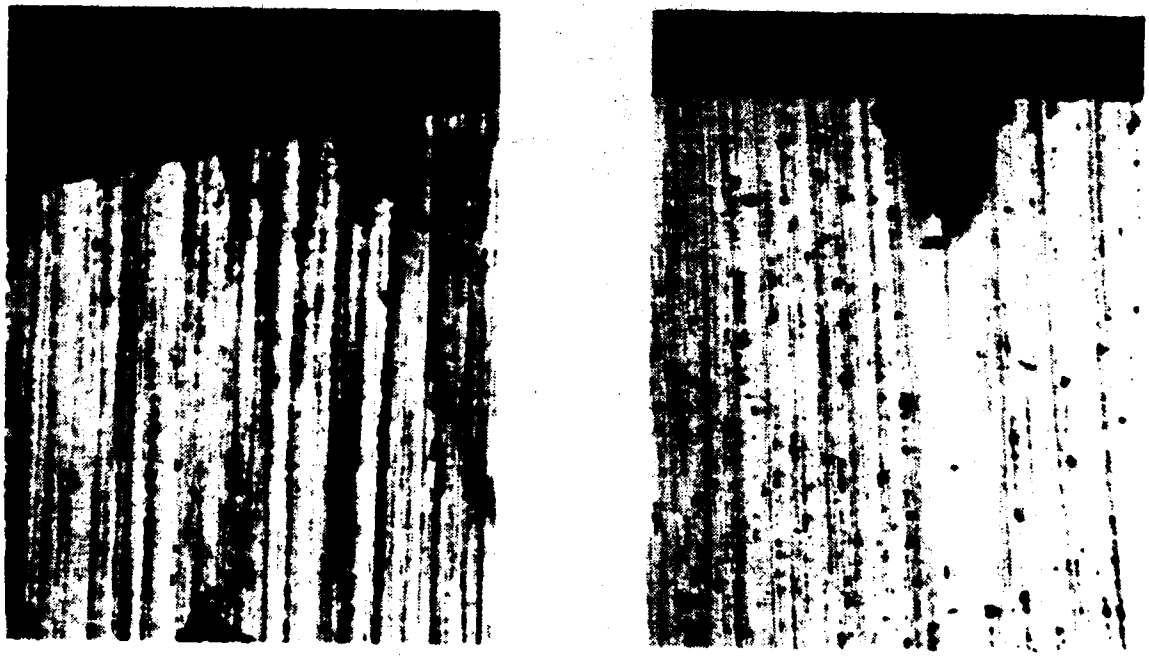

Figure 5. Photomicrographs of 7075—T651 A1 Alloy C-Rings in T6 and RRA Conditions after 28 Days Alternate Immersion Corrosion Tests in 3.5% NaC1 Solution at a Stress Level of 25 KSI (172 MPa) Showing Cracks in T6 and only Pitting in RRA Specimens.

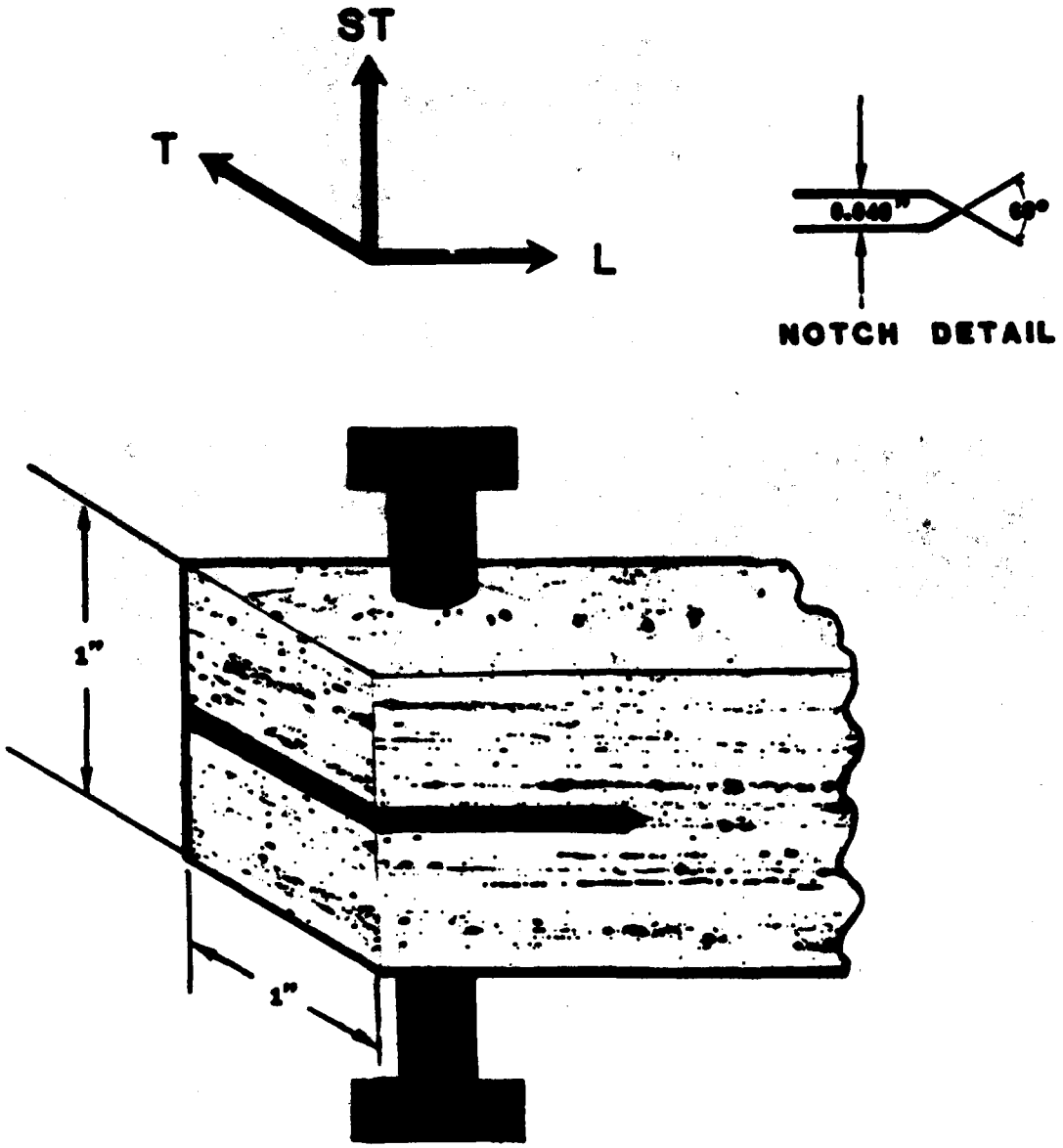

Figure 6. Double Cantilever Beam Specimen For S C C Testing.

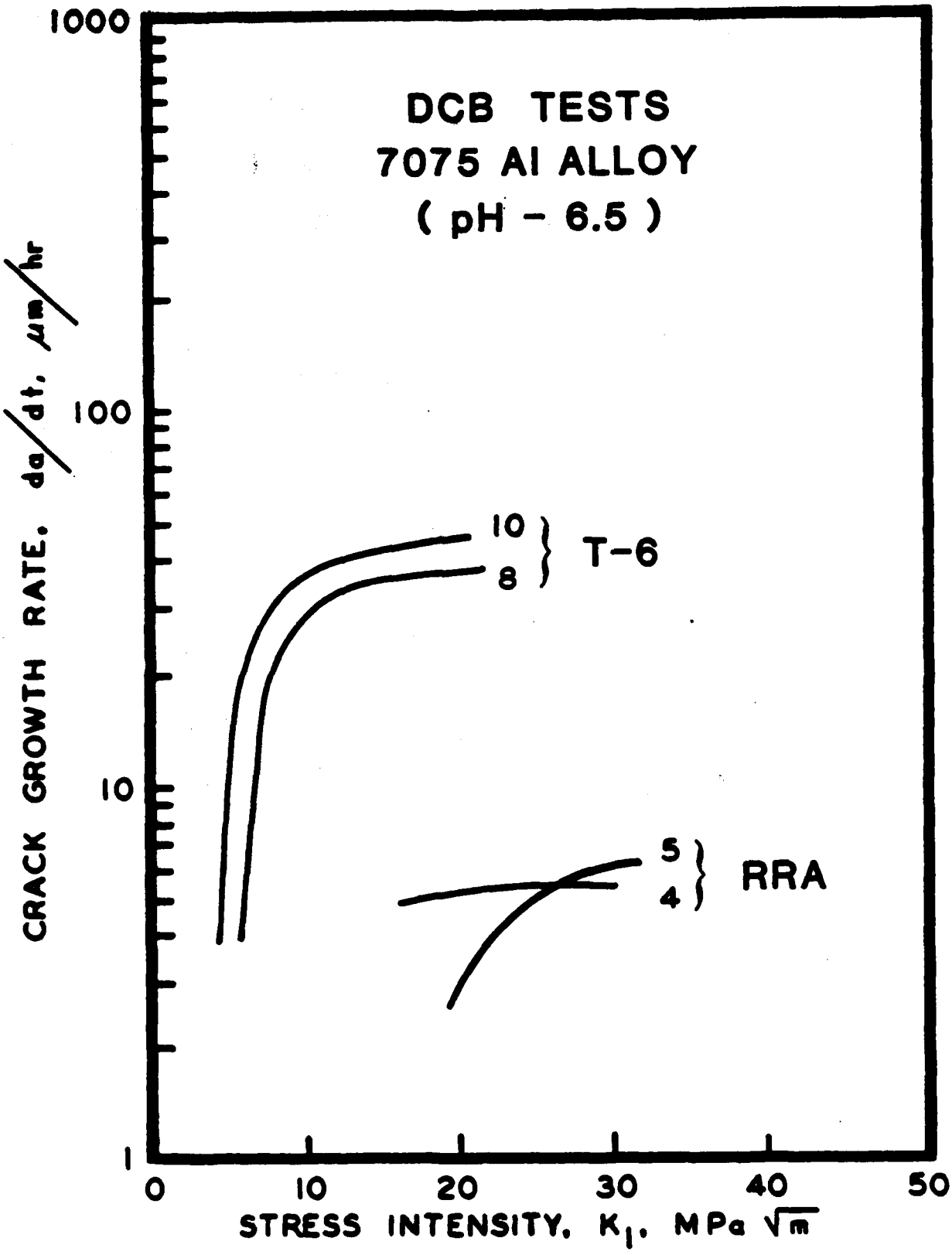

Figure 7. Comparison of Crack Growth Rate and Stress Intensity Data for 7075-T651 and RRA Double Cantilever Beams Specimens in the Notch Exposed Condition with 3.5% NaCl Solution At pH 6.5.

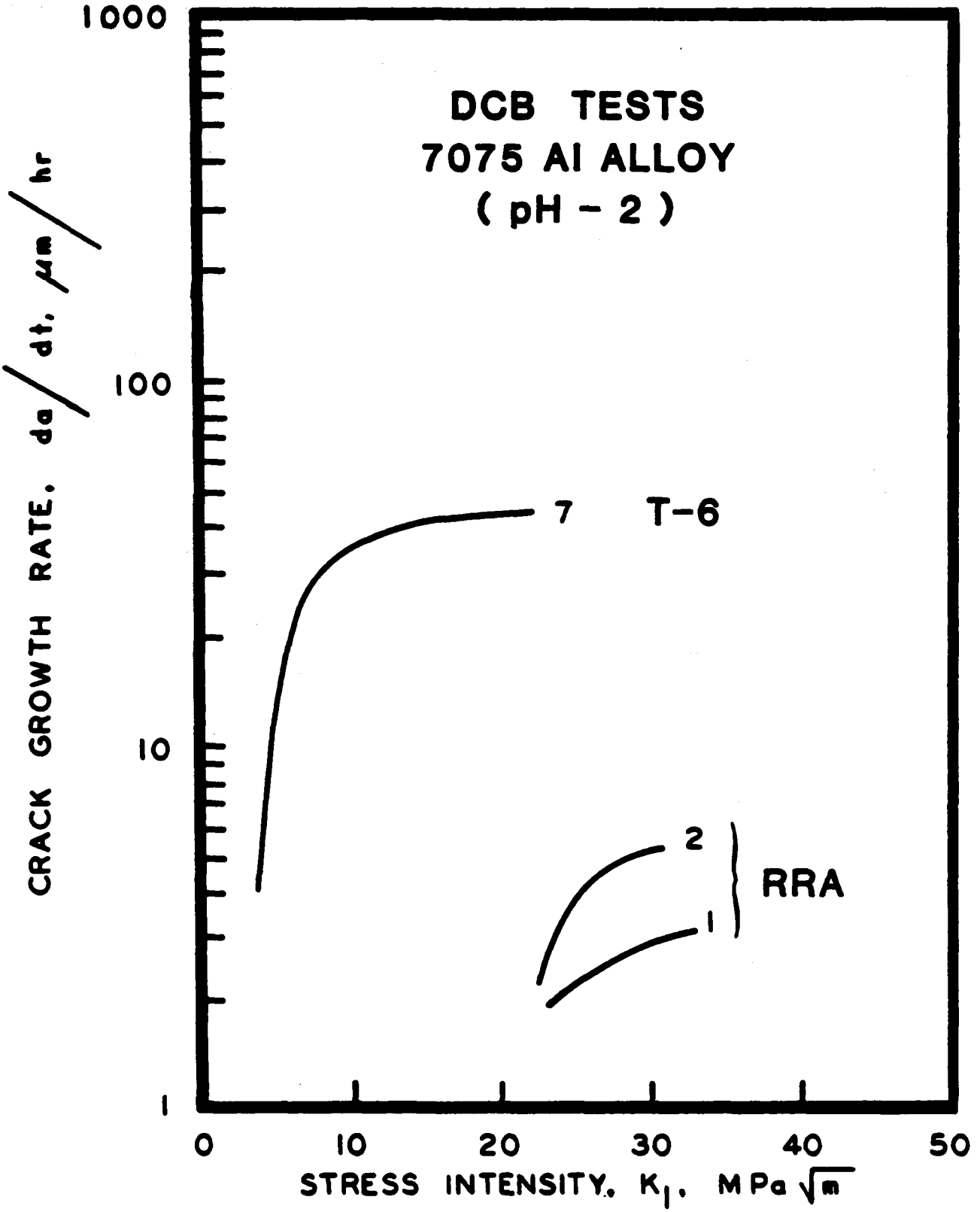

Figure 8. Comparison of Crack Growth Rate and Stress Intensity Data for 7075–T651 and RRA Double Cantilever Beam Specimens in the Notch Exposed Condition with 3.5% NaC1 Solution At pH 2.

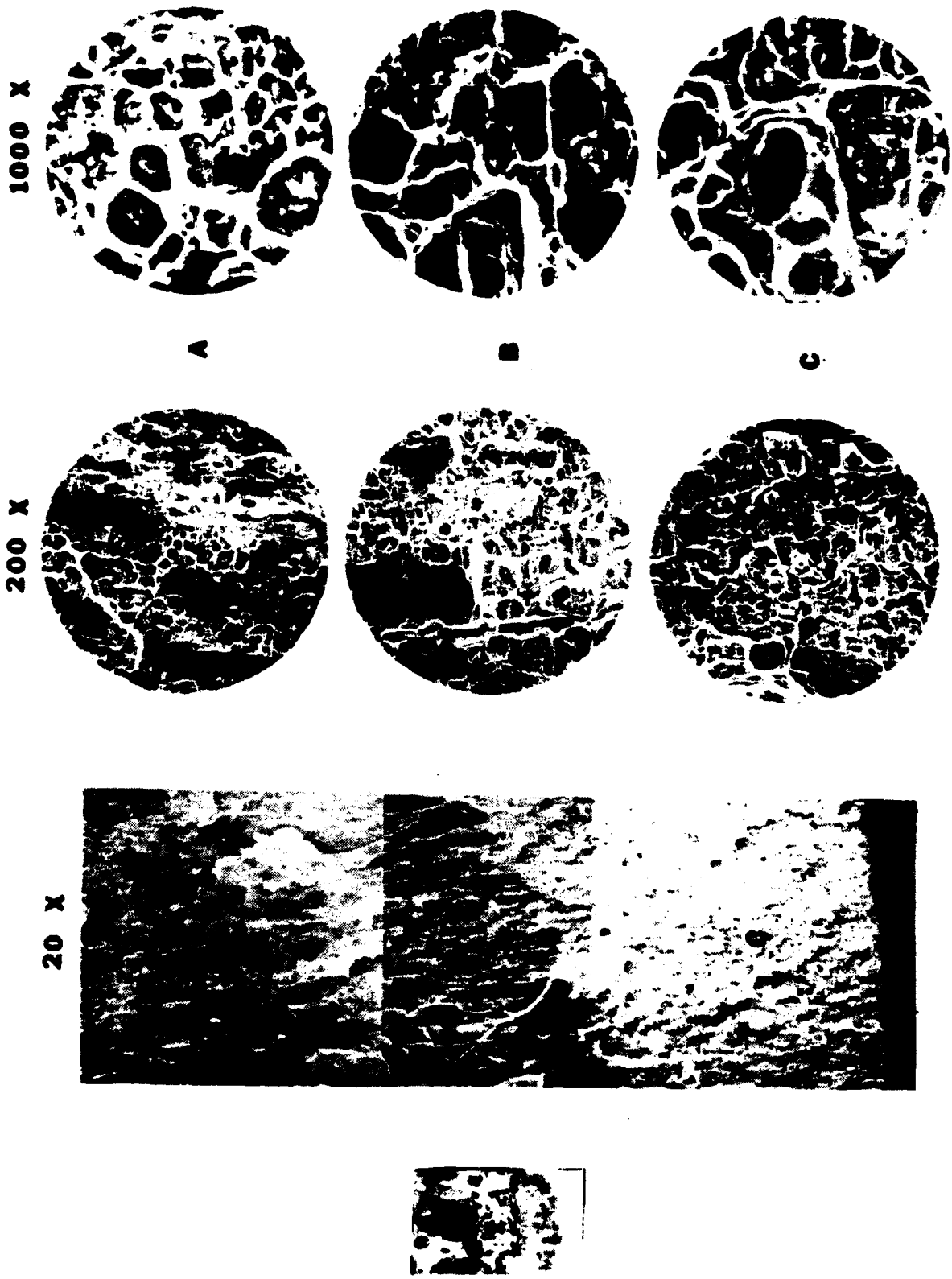

Figure 9. SEM Fractographs of the RRA Treated 7075–T651 A1 Alloy DCB Specimen after the Test At pH 2.

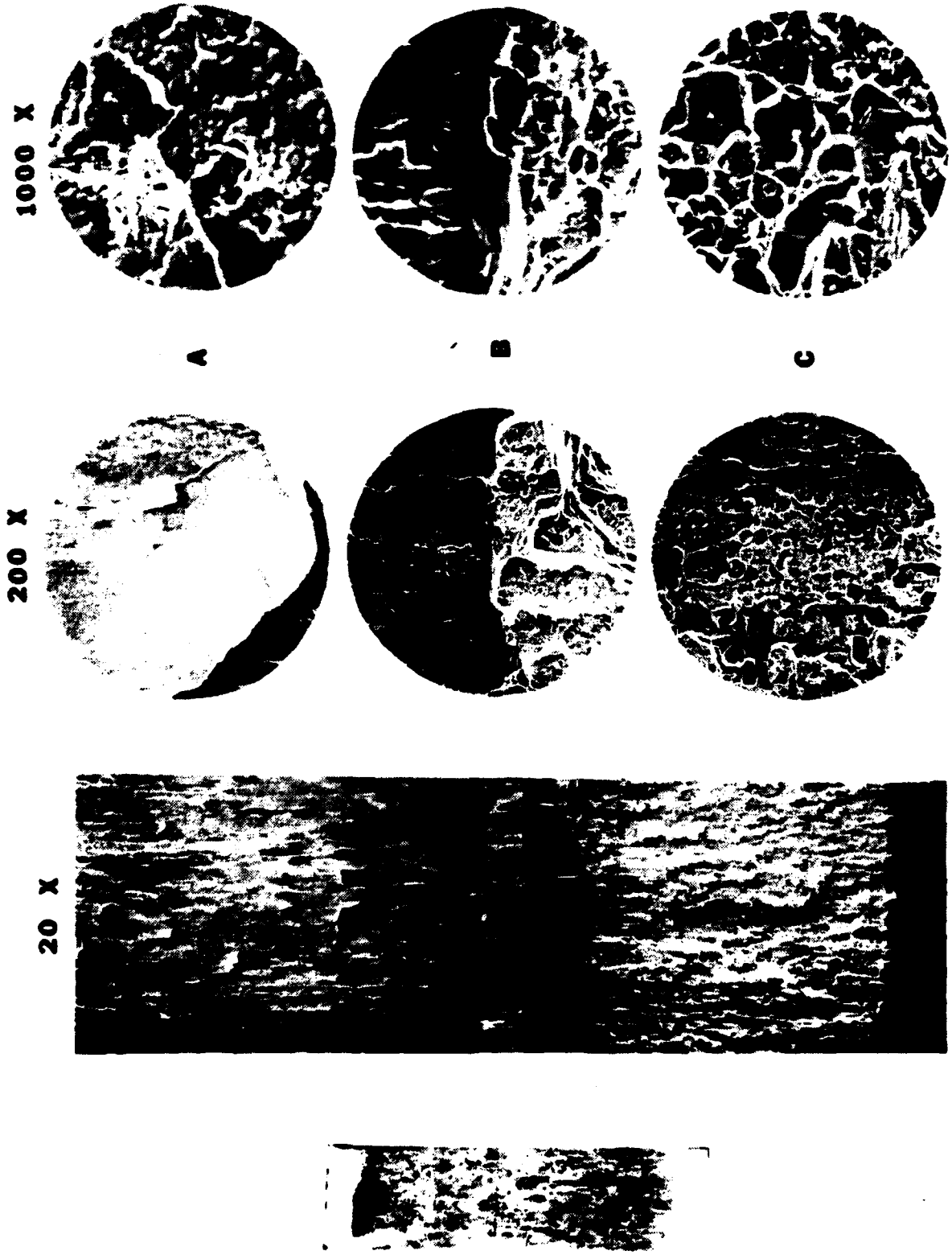

Figure 10. SEM Fractographs of the 7075–T651 A1 Alloy DCB Specimen After the Test At pH 2.

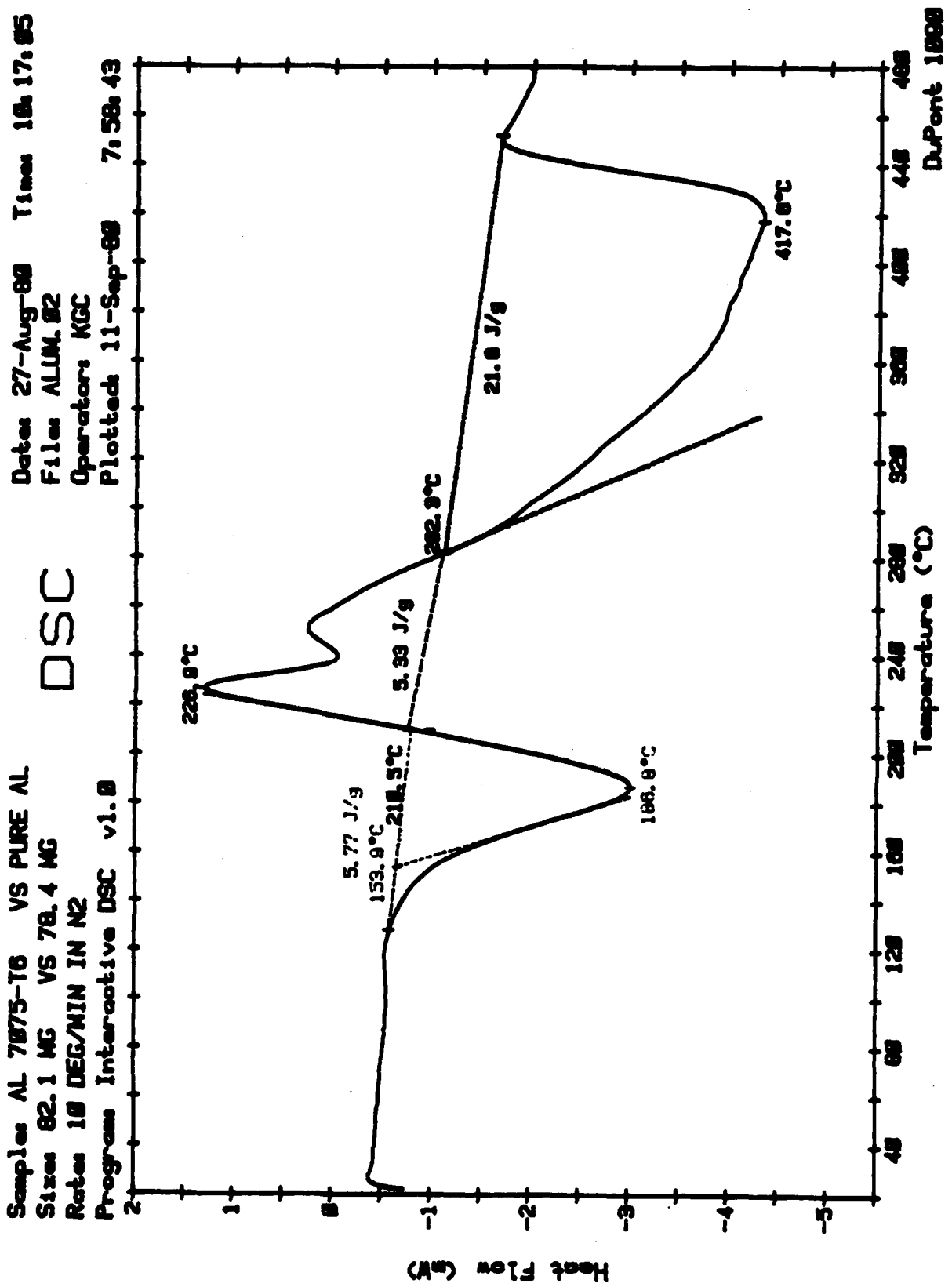

Figure 11. Differential Scanning Calorimetric (DSC) For 7075-T651 A1 Alloy.

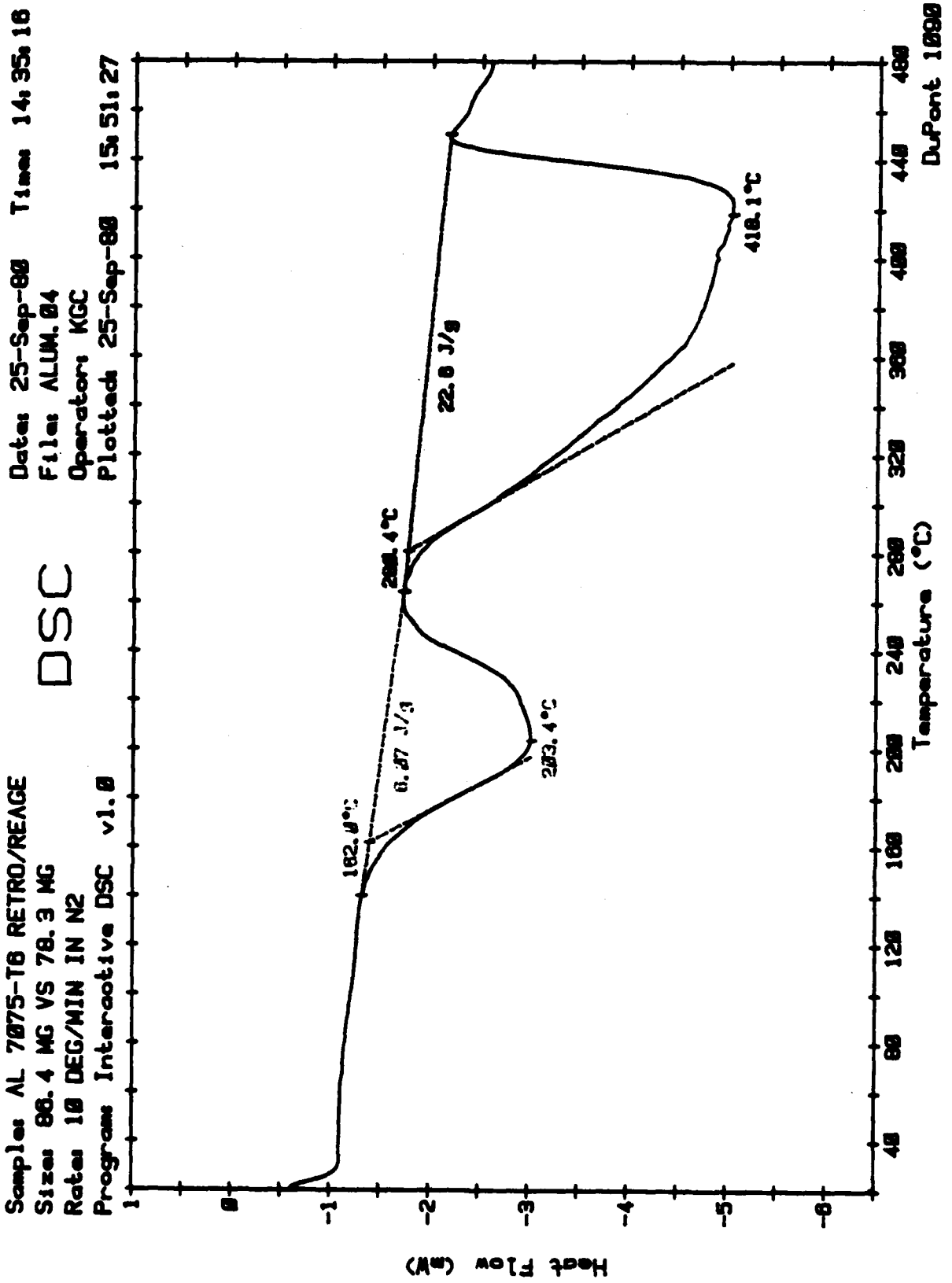

Figure 12. DSC Trace For RRA Treated 7075–T651 A1 Alloy.

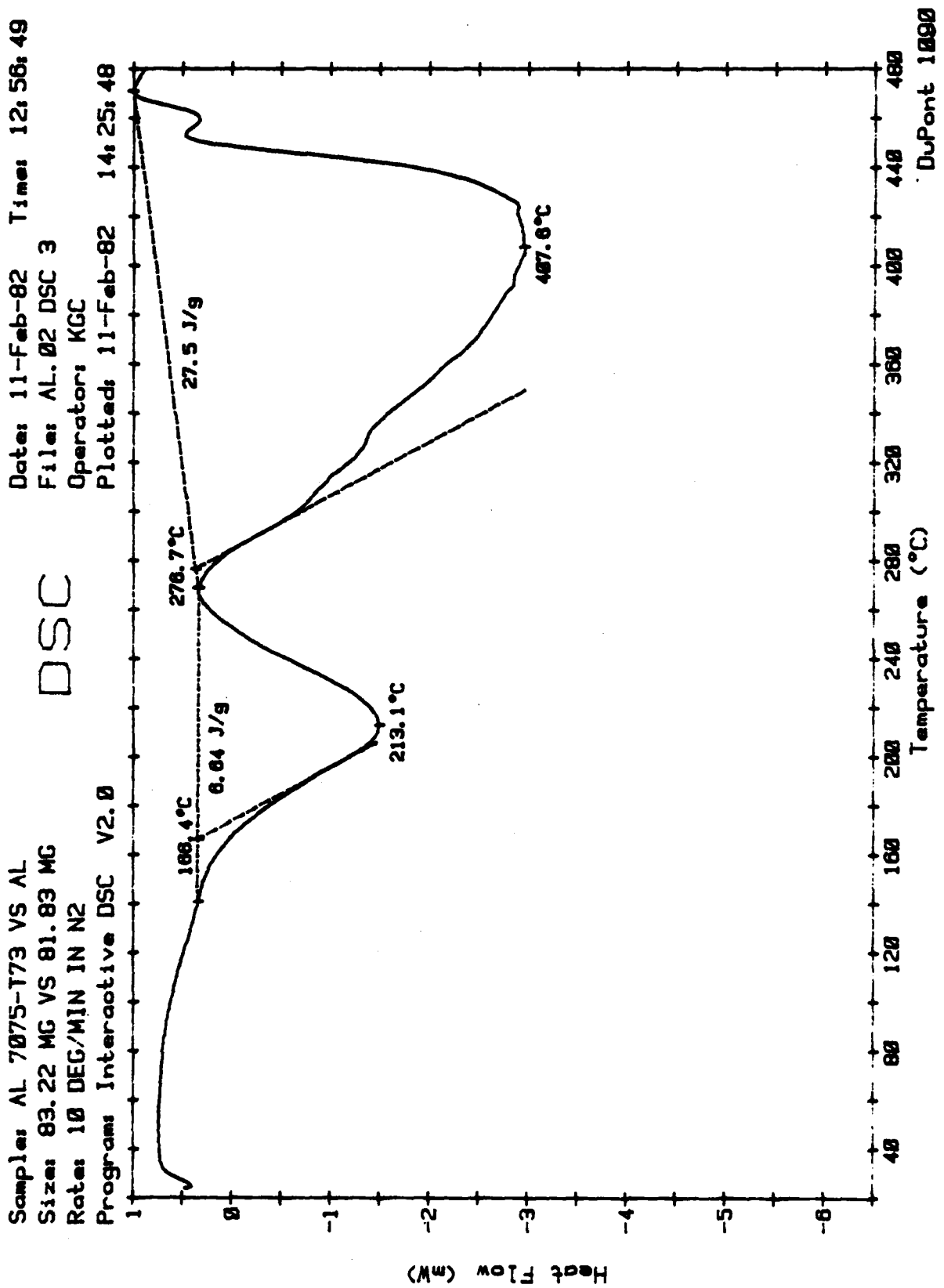

Figure 13. DSC Trace For 7075-T735 A1 Alloy.

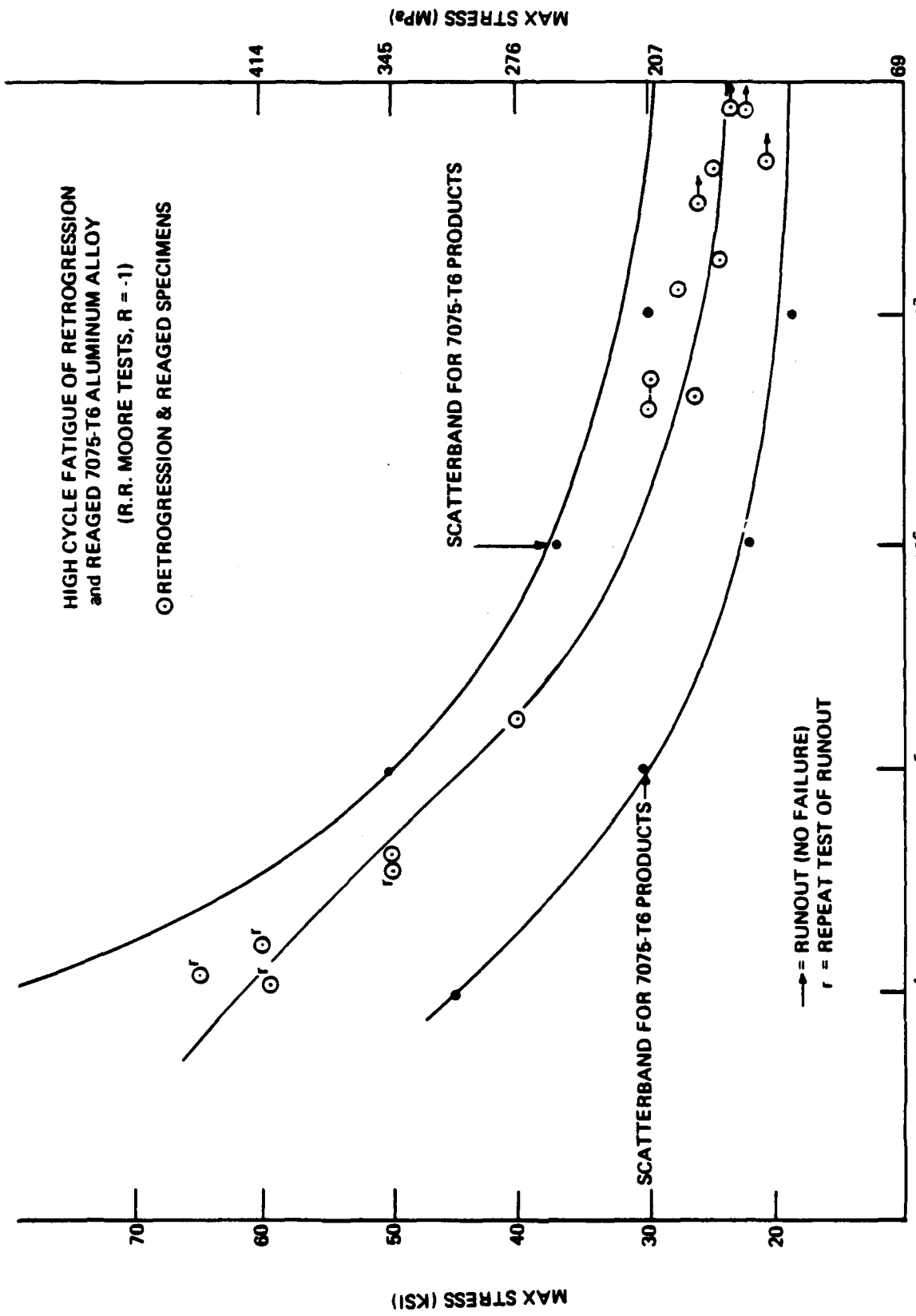

Figure 14. Comparison of Rotating Beam Fatigue Test Results for 7075–T651 Plus RRA Wing Data Range for 7075 T6 (Reference h).

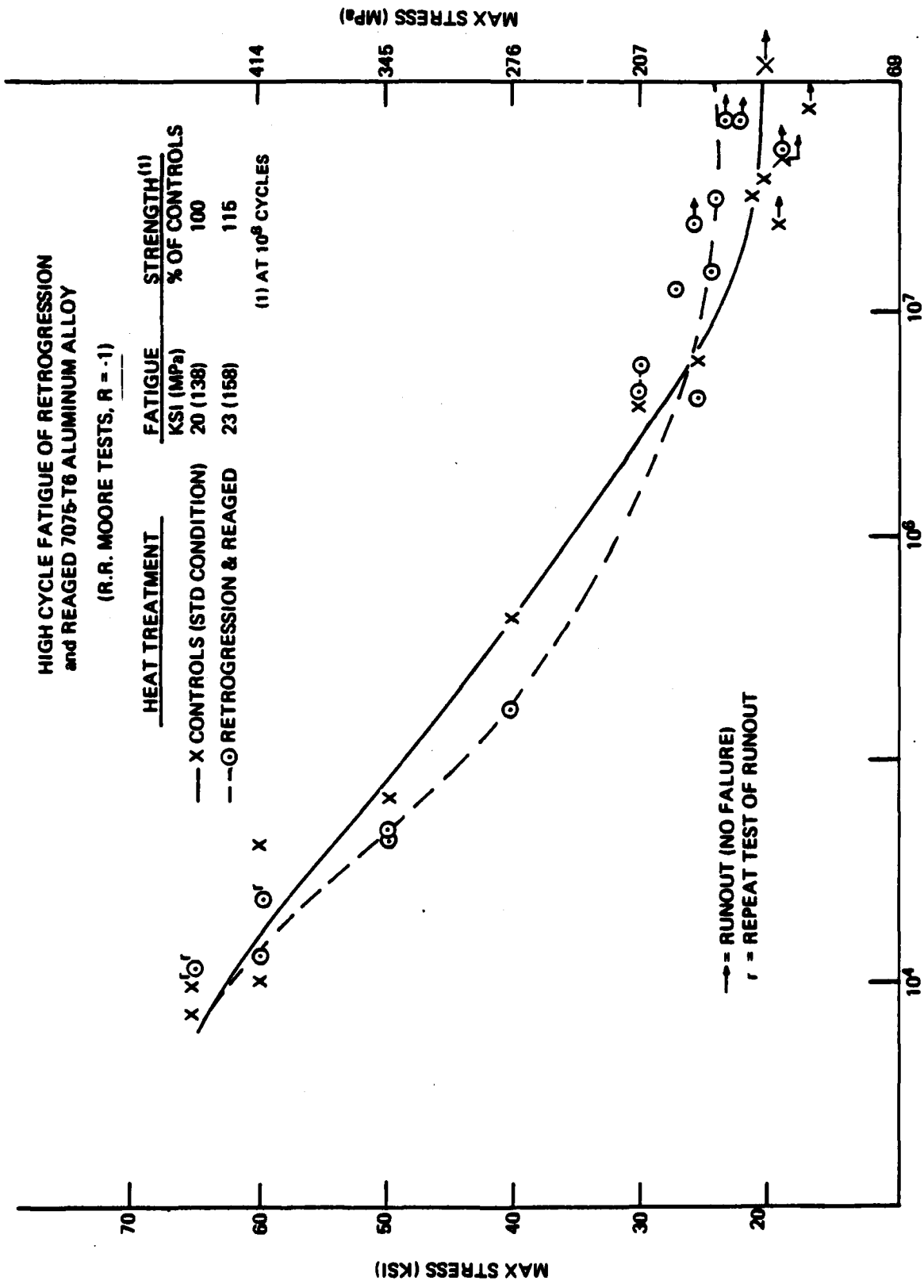

Figure 15. Comparison of Rotating Beam Fatigue Tests Results for 7075–T651 and RRA Material.

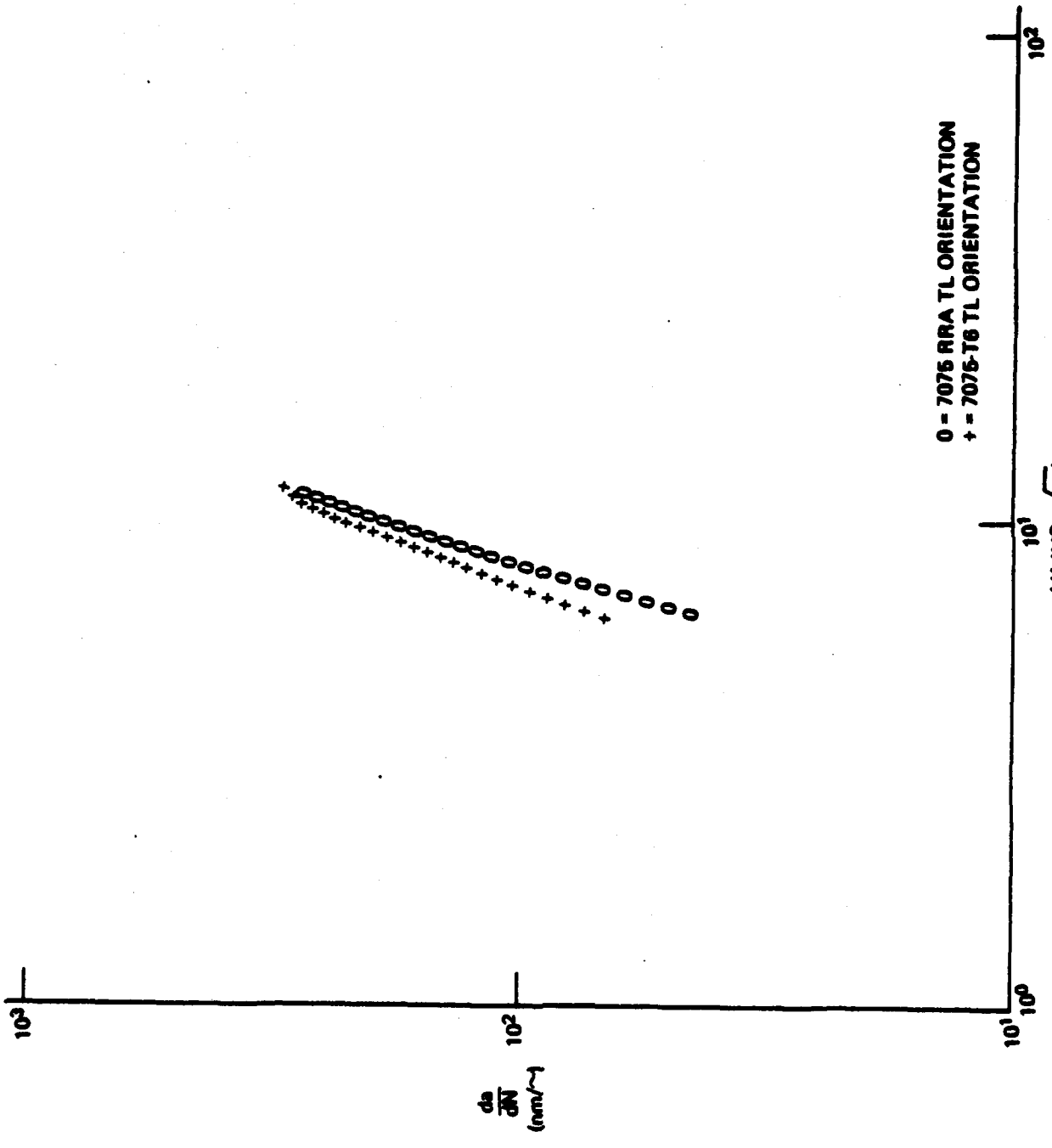

Figure 16. Comparison of Fatigue Crack Growth Rate Test Results for 7075–T651 and the RRA Treatment in the TL Orientation.

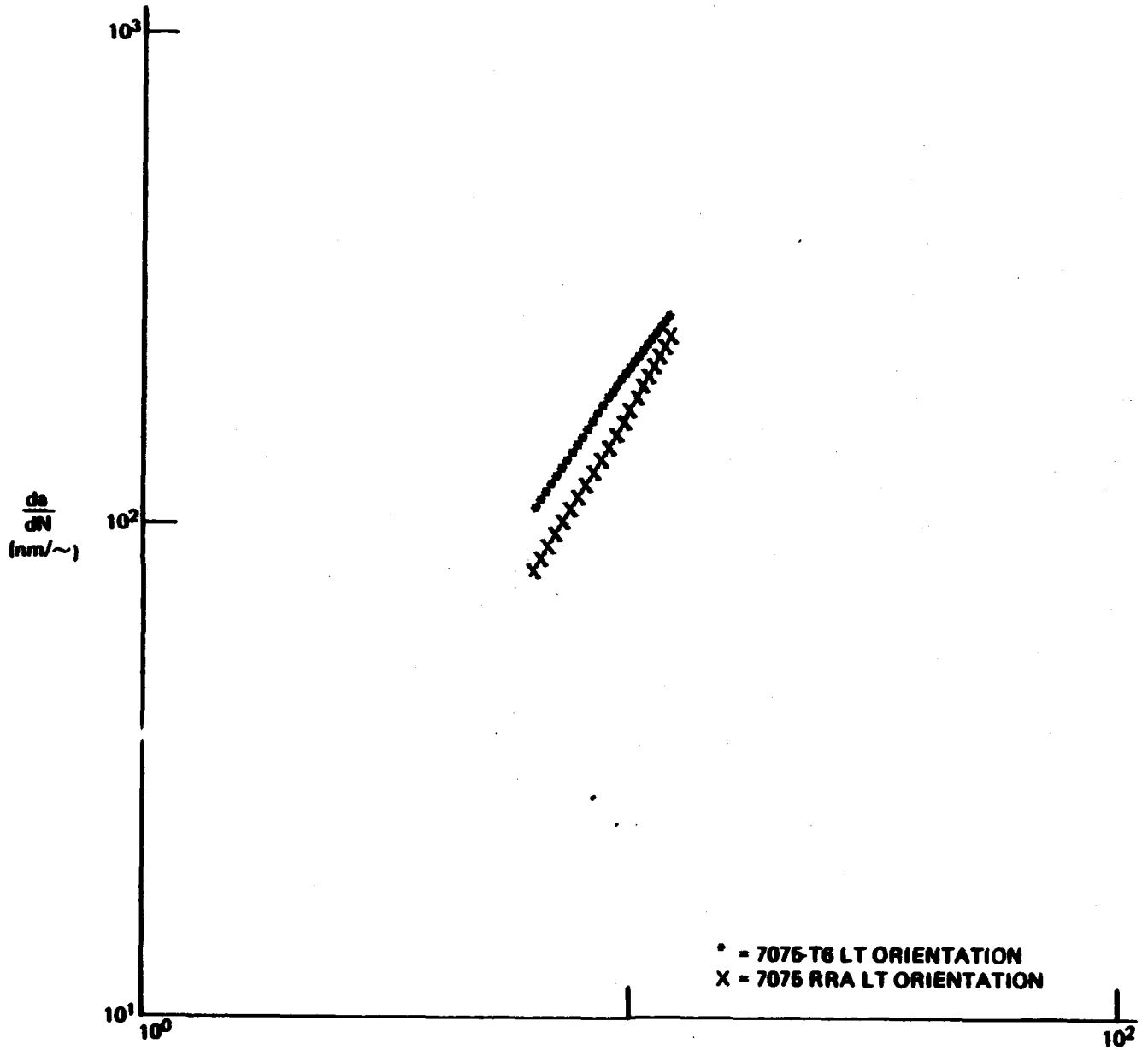

Figure 17. Comparison of Fatigue Crack Growth Rate Tests Results for 7075–T651 and the RRA Treatment in the Lt Orientation.

THIS PAGE INTENTIONALLY LEFT BLANK.

APPENDIX A

DETERMINATION OF STRESS CORROSION CRACK GROWTH RATE

(DCB TEST)

APPENDIX A

Determination of Stress Corrosion Crack Growth Rate (DCB Test)

Stress intensity (K) is calculated from the equation:

$$K = \frac{VEH\,[3H\,(a+0.6H)^2 + H^3]\,1/2}{4[(a+0.6H)^3 + H^2a]} \quad \text{---------- (1)}$$

Where V = Crack opening displacement measured at load line after pop-in crack.

H = beam thickness (specimen max height)

a = crack length measured from load point (Center line of loading bolts)

E = Youngs Modulus

da/dt is plotted as a function of K.

The experimental data consisted of crack length measurements as a function of exposure time. It was found that a Parabolic function resulted in the best curve fit. The data was reduced by an appropriate program to the following form:

$$a = A + Bt + Ct^2 \quad \text{------ (2)}$$

a = crack length

t = time

Where A, B, C etc. are constants $\frac{da}{dt}$ was determined by utilizing a modified program designed to give values for the following expression

$$\frac{da}{dt} = B + 2Ct \quad \text{---------- (3)}$$

The data reduction for the crack length are summarized in Table 1.

TABLE A-1

EQUATIONS FOR THE CRACK LENGTH RESULTING FROM THE PARABOLIC FIT

Specimen	Heat Treatment	Test Condition pH	Direction of Stress	Equations for Crack Length Growth vs. Time
1	RRA	2	S–T	$a = 0.51 + 3.02 \times 10^{-3}t - 3.5 \times 10^{-7}t^2$
2	RRA	2	S–T	$a = 1.51 + 5.29 \times 10^{-3}t - 1.65 \times 10^{-6}t^2$
3	RRA	2	S–T	$a = 2.68 + 5.66 \times 10^{-3}t + 4.0 \times 10^{-7}t^2$
4	RRA	6.5	S–T	$a = 3.4 + 5.42 \times 10^{-3} - 1.3 \times 10^{-7}t^2$
5	RRA	6.5	S–T	$a = 2.05 + 6.4 \times 10^{-3}t - 1.14 \times 10^{-6}t^2$
*6	T-6	2	L–T	$a = 0.921 + 2.56 \times 10^{-3}t - 3.20 \times 10^{-6}t^2$
7	T-6	2	S–T	$a = 7.45 + 4.5 \times 10^{-2}t - 1.13 \times 10^{-5}t^2$
8	T-6	6.5	S–T	$a = 8.99 + 3.9 \times 10^{-2}t - 1.17 \times 10^{-5}t^2$
*9	T-6	6.5	L–T	$a = 0.705 + 4.4 \times 10^{-3}t - 1.3 \times 10^{-7}t^2$
10	T-6	6.5	S–T	$a = 8.08 + 4.86 \times 10^{-2}t - 1.24 \times 10^{-5}t^2$

There was an excessive amount of scatter in the data.

*L–T Long Transverse

S–T Short Transverse

DISTRIBUTION LIST

REPORT NO. NADC-84096-60

AIR TASK ZF61-542-001
Work Unit No. ZM501

	No. of Copies
NAVAIRSYSCOM (AIR-0004)	7
2 for retention	
1 for AIR-31	
1 for AIR-5302	
1 for AIR-5304	
1 for AIR-53048	
1 for AIR-530484	
ONR, London (CDR Strada)	1
Chief of Naval Research (Code 471)	1
Chief of Naval Technology (Code 0715)	1
Naval Research Laboratory, Washington, DC 20375 (E. McCafferty)	1
NAVAIREWORKFAC, NAS, Alameda (Code 340)	1
Jacksonville (Code 340)	1
Norfolk (Code 340)	1
North Island (Code 340)	1
Pensacola (Code 340)	1
MCAS, Cherry Point (Code 340)	1
CHIEF, MATERIALS AND PROCESSES AT:	
Grumman Aerospace Corp., Bethpage, L.I., NY	1
Lockheed-California, Burbank, CA	1
Lockheed-Georgia, Marietta, GA	1
MCIC, Battelle Memorial Institute, Columbus, OH	1
National Bureau of Standards, Washington, DC	1
McDonnell Aircraft Co., St. Louis, MO (H. Turner)	1
Army Materials and Mechanics Research Center, Watertown, MA (M. Levy)	1
WPAFB (AFWAL/MLLN and AFWAL/MLSA), Dayton, OH	1
DTIC	12

END

FILMED

9-85

DTIC